

In this document, we respond to the comments of reviewer 1 one by one. Whenever some entirely new text has been added to the manuscript, it has been added in italics and in red below.

In the proposed revised manuscript, which is added at the bottom of this document, the textual changes have been added in red.

Reviewer 1 – Evan Miles

The study by Van Tricht et al presents a set of experiments to find the best image processing approach to resolve glacier surface mass balance from high-quality multi-year UAV measurements. The study is generally well implemented and seems to produce an approach to derive reasonable distributed SMB estimates based on the correspondence with stake measurements, suggesting filtering of thickness and velocity gradients, as well as direct flux divergence values, over a multiple-ice-thickness length scale. The study also highlights the importance of high-accuracy ice thickness data.

This is a welcome contribution to the field, as implementations of the continuity approach have come increasingly into vogue over the past few years, and UAV surveys have made high-precision topographic data a routine aspect of glacier monitoring. This study particularly offers the potential of deriving spatially-distributed flux divergence values, rather than based on glacier segments or for a single point. It is especially nice that authors have made use of a great set of field data to evaluate their model well; this is an important and challenging step. The manuscript is nicely written and the work is presented well. I do have a number of comments for the authors, including a few more substantial methodological concerns which the authors should consider, particularly with regards to the choice of filters and assumptions/effects thereof.

We would like to thank the reviewer for taking the time to provide a useful, comprehensive, and detailed review of our paper. We have addressed all comments below and updated the manuscript accordingly where needed. We believe this has strongly improved the quality of the research.

General comments:

[RC1.GC1] It is not apparent that the authors have evaluated whether the filtering has significantly impacted the total net volume change (or net flux divergence) – is mass conserved after all the filtering? Essentially, neither the variable box average filter or the exponential decay filter are conservative – they change the local and non-local mean values. I think it is likely that this does not result in a significant difference in the total volume loss or total flux divergence, but the authors should evaluate whether the difference falls within the uncertainty of the underlying data, or whether the filtering has internally broken mass conservation.

The reviewer raises an important subject here. We have addressed this in the revised manuscript. To provide for conservation of mass concerning the ice flux divergence, we ensured that the net

flux divergence before and after the filtering is the same by multiplying the filtered values by the ratio of the net flux divergence before and after filtering. This information is added in the text in lines 409-410:

“To provide for conservation of mass, the filtered result in each grid cell is multiplied by the ratio of the net flux divergence (sum of all ice flux divergences) before and after filtering.”

It is worth noting that the differences are small, so the results are minimally affected. The ratio is 0.93 for 2-17-2018, 0.91 for 2018-2019 and 0.92 for 2019 -2020.

[RC1.GC2] I found it strange for all values to be in ice equivalent! This avoids the difficult topic of density (less difficult in the ablation area) but I think it would be better to make an assumption, present your results in the standard unit, and then briefly mention this problem in the discussion (future work/opportunities/needs).

We understand this comment of the reviewer. However, the direct unit inferred from our approach is the surface density. In the ablation area, where the surface consists entirely out of ice, the latter is ice density. Further, because in the continuity equation, two out of three terms are in ice density, we kept the units in ice density. A conversion to water equivalent would require a single ice density assumption for the area under consideration. We added a section in the discussion in which we elaborate on the density considerations in lines 768-772:

“To convert the results presented here to the conventional unit of mass balance, assumptions must be made for density. In the ablation area, to which our study area was limited, the SMB could have been converted directly to metres of water equivalent using an average ice density such as 900 kg/m³. However, when the presented method would be applied to for example the accumulation area, specific attention is required for each quantity of the continuity equation (Miles et al., 2021).”

[RC1.GC3] One of the filtering steps (for the dH/dt data) aims to correct apparent surface changes due to advection of surface features. I would recommend that the authors examine the flow corrections of e.g. Brun et al (2018) which are a more appropriate approach to resolve this problem, but requires switching from an Eulerian to Lagrangian frame, which is anyhow more appropriate for comparing to a stake.

We are aware that with our approach we may have filtered out also relevant measured changes. Because the method of flow correcting the DSMs, as for example used by Brun et al. (2018), is physically more justifiable, we agree with the different reviewers to apply this method. We added the explanation in lines 287-291:

“The different DSMs are treated considering the motion of the ice, following the method applied in e.g. Brun et al. (2018). This method consists of projecting each point on the glacier back to its original position in the previous year, based on the local velocity in x and y direction and taking into account

the vertical displacement produced by flow along the longitudinal slope. The latter is determined by taking the average slope over all the different years for which a DSM was made, smoothed with a Gaussian filter.”

The results have changed little, perhaps because the stakes are in stable areas of the glacier, so the flow corrections and our filter method do not differ much. However, the pattern of the SMB has become less homogeneous, due to artefacts in the flow correction method. This is clarified in the text in lines 596-600:

“The presence of certain irregular patches with a smaller or larger SMB is caused by artefacts in the flow correction method (see section 3.2 and Figure 6d). This is because the flow correction method cannot trace all displacements exactly (rocks fall over, crevasses deform, supraglacial melt streams are positioned on different locations etc.), and because the velocity field is not fully accurate, and the calculation of the longitudinal slope also affects the result.”

[RC1.GC4] For both velocity and thinning datasets, the authors have discarded data outside the glacier boundary, but they should instead use these data to empirically assess the quality of their results. Similarly, the combination of the ice thickness datasets is a bit awkward; it would make more sense to me to integrate all available bed elevation observations to produce an optimal ice thickness dataset. However, this may not be feasible for multiple reasons, and would require reprocessing nearly all datasets, so I can understand that the authors may wish to avoid that course.

Using the areas outside the glacier outline is definitely a useful way to measure the absolute error, in addition to the use of validation points which can specifically be used to measure the relative error and self-consistency of the DSMs. In the section where we describe the error based on the validation points (section 4.1), we added a text and figure in which we elaborate on the off-glacier variations in surface elevation changes (lines 468-477):

“Then, the accuracy of the surface elevation changes is assessed by comparing the elevation differences in rectangular areas outside the glacierized areas for two regions (see Figure 6), where the topography is assumed to be mostly stable (Yang et al., 2020). The histograms for the three different balance years in consideration show that most of the differences range between -0.2 and 0.2 m, which indicates that there is no large absolute offset between the DSMs of the different years (Figure). For region 2, we find a larger standard deviation (SD) for the 2017-2018 difference which appears to be caused by a small horizontal shift which produces larger elevation differences (both negative and positive) in this steeper area. For the gentler sloping glacier surface, the effects are negligible. The larger SD for the 2019-2020 difference in region 1 is caused by an area where a part of the bare surface was eroded by a melt river, producing a tail of negative elevation differences. In general, the above analysis reveals that the vertical uncertainties resulting from the DSM differencing are limited.”

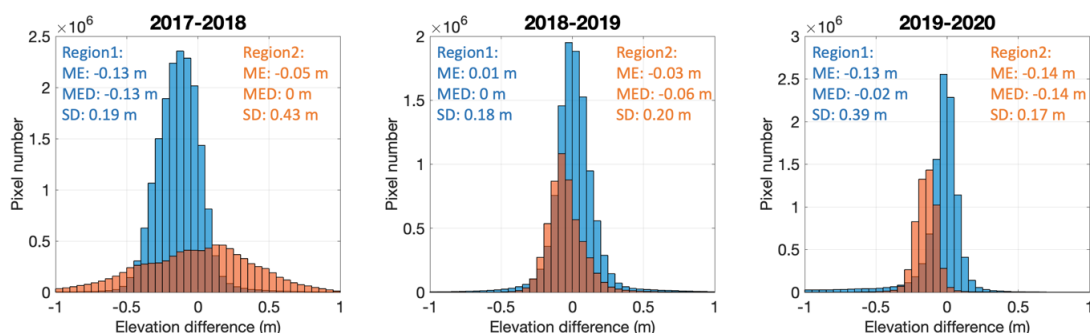


Figure 5. Histograms of elevation differences for the different balance years considered. The mean error (ME), median error (MED), and standard deviation (SD) are added for each region.

as well as concerning the surface velocity in line 310:

“after verifying average zero displacement for stable areas outside the glacier”

Concerning the ice thickness datasets, indeed, both datasets differ substantially, although the patterns are similar. Our measurements in 2020 (which lie between the two datasets) showed that neither one of the two could be dismissed. Therefore, we opted to take the average ice thickness as our main dataset for this study. Furthermore, extensive tests with both datasets encouraged us again to use the average ice thickness. We clarified this in the text in lines 711-716:

“We therefore conducted some additional tests with both (THIZ and THIL) individual ice thickness datasets and for different combinations. For Pers glacier, the Langhammer dataset proved to be slightly better, while for Morteratsch, the Zekollari dataset performed better. But in general, all combinations tested gave more poor results, which encouraged us to use the average ice thickness in this study. It should be mentioned that the above analysis is valid for the glacier wide mean SMB deviations. For local point measurements, the uncertainty related to the used data, or the F-parameter, might be larger.”

[RC1.GC5] The justification of an exponential decay filter is not particularly strong, and I am concerned that the optimal distance results may be sensitive to the type of filter used. It would be worthwhile to consider other approaches or justify this choice (and its implicit assumption).

During the study, we conducted several tests with a mean, median, Gaussian and exponential filter. All with a constant size/variance/length scale over the study area and with a variable value for these parameters (depending on local ice thickness, local surface velocity etc). The exponential filter came out as the one with the best results for the smallest distance over which to filter, closely followed by the Gaussian filter. This also means that the ice flux divergence field which is

obtained after exponential filtering still contains the most detail, unlike filtering over very large distances which smears out the entire flux field. We agree with the reviewers that an exponential filter gives the local grid cell the most weight, but with a large length scale (which proved to be necessary – several times the local ice thickness), the surrounding cells also get a significant contribution. In addition, the tail of an exponential filter decreases more slowly towards 0, so that grid cells further away from the grid cell under consideration retain more weight than with a Gaussian filter.

A box method such as a mean or median filter gives equal weight to cell irrespective of their distance from the point in consideration. The issue we observed with these filters is that the effects of local phenomena (such as an ice fall or such as an acceleration in the glacier flow) are spread out uniformly when they are applied over larger distances which would imply that there would be no localized peaks in the flux divergence field. An exponential decay filter preserves this variation while filtering enough to get a smooth solution. Indeed, the local grid cell has the largest effect, but its value is “muted” by the spatial averaging. Our tests with the Gaussian filter showed only slightly less good results for the same/somewhat larger spatial scales. A Gaussian filter could therefore be an alternative, albeit with slightly less good results for this study.

To make this clearer in the text, we added some sentences to clarify our choice for the reader in lines 375-377

“In this way, the effects of local phenomena (such as an ice fall or an acceleration in the glacier flow) are spread out uniformly when these filters are applied over larger distances, which implies that there are no localized peaks in the flux divergence field.”

and 758-760:

“Other filters such as a mean filter or a Gaussian filter were explored, but all gave (slightly) less accurate results. However, our tests with a Gaussian filter showed only slightly larger errors for similar spatial scales. A Gaussian filter could therefore be a possible alternative to the exponential filter.”

Minor comments:

[RC1.1] L26-L27. Suggest ‘...several times the local ice thickness, accomplished in this study using an exponential decay filter.’ There are several ways to consider the larger scale variations in stresses; your study nicely points to the exponential decay filter as one good approach.

We updated the text in the manuscript.

[RC1.2] L42. I’d suggest spelling out interpolation here and in the conclusions. Not so many letters but improves readability.

Done.

[RC1.3] L51-53. Suggest citing Berthier et al (2012) or similar studies here. Also a key point is that even if one corrects for ice flow, assumptions regarding ice density are needed to assess glacier mass balance, which are not the same assumptions as for the glacier scale (e.g. Huss, 2013).

Thank you for suggesting this paper. We included this reference.

[RC1.4] L60. There are many other relevant references here, and you can't be exhaustive, but see also Brun et al., (2018) and Wagnon et al (2020).

We thank the reviewer for suggesting this literature, which we added.

[RC1.5] L64. I'd be more explicit that many studies reduce the problem by using flux gates. I suppose this is a one-dimensional reduction and indeed smoothing, but it's also an entirely different kind of data processing.

We agree with the reviewer to make this more explicit and added a sentence to this section.

[RC1.6] L152. Is this the difference in SMB values or the rate?

This difference corresponds to the difference in rate. We added this to the manuscript.

[RC1.7] L171-183. The disagreement of the two thickness datasets is interesting and not terribly surprising. However, I am surprised that the authors have relied on the two modelled datasets (based on distinct field measurements and necessarily extrapolated using physical principles) rather than integrating the underlying field measurements of bed elevations in an updated ice thickness estimate. Surely this would result in a better consensus than the mean of two model results? This would allow you to also integrate your 2020 measurement(s).

See our answer in RC1.GC4.

[RC1.8] L188. These values differ by 18-24%

Modified.

[RC1.9] L255. Did you look at your off-glacier dH measurements (bias and standard deviation) at all? As with velocity, these provide an important measurement of error.

See our answer in RC1.GC4

[RC1.10] L260. Yes, these undulations are quite annoying from a geodetic perspective (and they mostly cancel one another out) but I find it strange to filter them out, when you could instead flow-correct the DEM (or underlying point cloud) using your velocity data (see Brun et al, 2018). An important test for this filtering is whether volume change is conserved before and after – do the volume-change measurements before and after the filtering equate? They are likely to be very close, but bear in mind that you are eliminating real volume changes; this is a good reason to consider warping your DEM to correct for glacier flow.

See our answer in RC1.GC3

[RC1.11] L277. Why is 25 in the denominator here? Should this be delta-x?

Corrected.

[RC1.12] L294. Please indicate what ImGRAFT settings you used, which correlator, etc, just for replicability

We have added this information in the text in lines 299-301:

“Specific settings for the template matching of ImGRAFT are the use of the orientation correlation (OC) method and a large search height and search width of 200 m, to guarantee that all possible areas are covered.”

[RC1.13] L303. Are the glacier outlines from a standard source (which?) or did you digitize them yourself?

The glacier outlines were manually digitized based on drone and satellite images. We included a sentence to clarify this in lines 312-313:

“The latter are manually digitized based on drone and satellite images and correspond to the end of the summer of every balance year under consideration.”

[RC1.14] L303. It's fine to remove them for your filtering, but the off-glacier velocity vectors give you an important metric of velocity uncertainty!

See our answer in RC1.GC4.

[RC1.15] L304. Do you median filter the u and v components or the speed (and direction)?

We filtered the u and v components and we added this in the text in lines 313-314:

“velocity components that deviate too much from the surrounding grid cells”

[RC1.16] L357. These studies don't really 'resample' to a lower resolution, they are instead resolving the flux across a gate or set of gates.

We agree and reformulated this in the text and we added a reference to Seroussi et al., 2011.

[RC1.17] L367. The choice of an exponential decay filter is interesting! I'm not fully convinced that an exponential is the best choice but neither is it a bad filter – have you tested or considered other filters for this? Unlike others (Gaussian, Weibull, mean/median), the exponential decay filter considers the closest observations to be the best estimate, giving the local value the highest weight. Do you have a reason to assume this to be the case? For instance, a block mean/median (as used for the dh/dt) would consider all nearby measurements to be a reasonable estimate. I see the exponential decay for a perturbation of ice thickness, but this is really the inverse process, no? I mean, the noise in the flux divergence map (which should be shown somewhere, by the way!) is in part due to ice thickness/velocity errors and in part due to the far-field longitudinal stresses. Did you test or consider other filtering approaches? For instance a Gaussian filter exhibits a similar distance decay, but considers any of the nearby estimates to be reasonable and weights them more or less equally.

L400. A concern here is that this filtering can internally 'break' conservation of mass. That is to say that the net flux divergence over your survey zone should equate to the flux into your survey zone; this should be the case with your gridded flux divergences, but after this filtering (which is not mass-conserving!) the net flux divergence (the integral of all pixel flux divergences) can change. Have you checked this? It is likely that the difference is within the uncertainty bounds of the flux into your lower domain, but this is a key problem with applying such filtering, and should be mentioned.

We thank the reviewer for this profound comment. Please see our answer in RC1.GC5.

[RC1.18] L403-407. The justification for applying both filters is not entirely clear to me from the text here. I see (later) that it does appear to improve the MAE results, but the text here could make the case more clearly for this.

Instead of applying one filter over a very long length, we found that applying two filters in a row over a smaller length improved the results and preserved more local phenomena. Furthermore, the filtering of gradients and/or the ice flux divergence for the glacier complex did not appear to be unconditionally the most optimal but the combination appeared to be. We clarified this in the text in lines 422-424:

“This tends to reduce the distance over which the filtering must be performed, which is favourable to preserve local variations.”

[RC1.19] L446. Looks like the comma wasn't meant to be here

Removed.

[RC1.20] L451. The exception of the debris-melt-reduction is the terminal ice cliff, as identified by e.g. Immerzeel et al (2014).

Thank you for this suggestion. We added a sentence with a reference to Immerzeel et al., (2014).

[RC1.21] L453-456. It is certainly possible that this pattern is due to avalanches, but it's worth nothing as well that this is probably the least-constrained part of your survey area; do you have GCPs or GVPs that high?

During fieldwork, we were able to place and measure GVPs and GCPs in this region. In doing so, we immediately noticed the presence of avalanche remnants. We are therefore strongly persuaded to attribute these positive elevation differences to avalanche nourishment. We added a map of the location of the GCPs to support this.

[RC1.22] L467. 'are occurring' -> 'are evident'

Agreed and replaced.

[RC1.23] L490. 'Constant box filter' -> not clear what you mean here. Do you mean the average value of a box (e.g. altitudinal or longitudinal bin)?

We are referring to a box average filter that has a constant size over the entire glacier surface. In this case it is not, as we vary the size according to the local velocity. We are therefore taking flow variations into account. Because we decided to flow correct the DEMs, this comment is no longer applicable. See our answer in RC1.GC3.

[RC1.24] L499. What is the physical meaning of $k=3$? Three times the local surface velocity? The spatial pattern looks nice, but in my mind it would be much better to flow-correct your DEM as in Brun et al (2018). This of course represents a shift from an Eulerian to Lagrangian frame.

We agree with the reviewer to flow correct the DEMs and calculate the surface elevation changes instead of filtering this data. See our answer in RC1.GC3.

[RC1.25] Figures 5 and 7. dh/dt has units of m per year.

Added.

[RC1.26] Figure 8. The black dashed line for VM is missing on the right panel. These would represent the ideal cross section to assess whether your filtering has conserved mass (flux through cross section = integral of flux divergence).

We thank the reviewer for pointing this out. We have added the line to the right plot.

[RC1.27] L540-542. I'd avoid the speculation about a slowdown; you would need very different data and methods to assess this meaningfully!

Removed.

[RC1.28] L553. Section reference to 4.3 within 4.3

Removed and replaced by 3.4.

[RC1.29] L605. This shows a problem of the filtering used here – the possible local ablation increase, if present in the dh/dt , has been filtered out.

We removed this section since in our new version we do include point M26 in the analysis.

[RC1.30] Figure 12. Very nice summary; the processing has produced some very nice results in terms of reproducing the stake measurements!

Indeed! The method works pretty well. We look forward to see the application of our method on other glaciers where similar data are available.

[RC1.31] L627. Nice to see this lateral heterogeneity highlighted, and very nice to see the local deviations from a linear ablation gradient. Can you indicate the standard deviation of SMB for elevation bins (for example) based on your data?

This is an analysis that we considered when writing the manuscript, but which we decided not to include in the text.

[RC1.32] L638. See e.g. van Woerkom et al, 2019.

Thank you for suggesting this reference. We included it.

[RC1.33] L648-655. This is a really nice result, because it highlights an area where the assumption $b=b_s$ breaks down. Do you have any measurements to isolate the surface and subsurface melt in these areas?

Unfortunately, we have no direct measurements in this area. During the fieldwork, we only observed large amounts of flowing meltwater at the bottom of these zones and a radial pattern of collapsing glacier walls.

[RC1.34] L667. I suggest making a note that the perturbation details will follow

Done

[RC1.35] L670. Is this MAE computed for all years' data or a single year?

The MAE is computed for all years. We clarified this in the text.

[RC1.36] L672-674. I'd appreciate a few more details about the implementation of these random perturbations. I can't tell if this is the equivalent of 'random Gaussian fields' or something else. Are the perturbation magnitudes also random (per realization? Per lump?).

Our perturbations are quite similar to random Gaussian fields but we deviate from them to the extent that the diameters of the patches are uniform for each perturbation. The perturbation magnitude is random per patch (=lump). We reformulated this in the text to clarify it in lines 684-686:

“For the analysis, the different input fields are perturbed using random patches with a diameter (uniformly distributed) between 50 m (local errors at grid level) and 500 m with perturbation values normally distributed with a standard deviation of half the error estimate.”

[RC1.37] L679. Do the perturbations of F, thickness, and velocity also follow the same ‘patch’ approach?

Indeed, all analyses are performed in the same way, using the patches. We reformulated this in the text to clarify this.

[RC1.38] Figure 14. It is clear that the thickness perturbations have had the greatest effect, but these were also the greatest perturbation (30% vs 10% for velocity), due to the uncertainty of the underlying dataset(s). As such, these results do not really correspond to ‘sensitivity’ but somewhat more the ‘uncertainty’ attributable to an individual dataset. I.e. if the thickness data had a 10% uncertainty, how would its associated errors compare to the velocity-associated errors?

The reviewer makes a good point here. With a 10% uncertainty, the contribution of ice thickness and speed would be about the same. However, what we wanted to show here is that in the derived field (and in the way we have done it) the ice thickness and associated uncertainty of that ice thickness influences the result mostly. Following the reviewer’s suggestion, we reformulated the title of this section into “uncertainty analysis”.

[RC1.39] L705. My only criticism here is that only the exponential decay has been tested, and I am not sure that it is necessarily better or conclusive, so I would suggest softening the language around ‘necessary’ to instead indicate that the exponential filter produces closer correspondence to stake measurements.

Although several filters have been tested, we agree with the suggestion to mention that our research showed that exponential filtering is a good choice, but it is not a necessity as other filters can likely have similar results. We clarified this in the text and refer also to our answer in RC1.GC5.

[RC1.40] L738. I'm missing a discussion section considering implications/recommendations/future work? Density considerations? How important are the lateral variations in SMB (how much impact do they have on mass loss overall?) etc.

This was also suggested by the other reviewers. In the revised manuscript, we added a discussion section (section 6).

Estimating surface mass balance patterns from UAV measurements on the ablation area of the Morteratsch-Pers glacier complex (Switzerland)

Lander VAN TRICHT^{1,*}, Philippe HUYBRECHTS¹, Jonas VAN BREEDAM¹, Alexander VANHULLE¹, Kristof VAN OOST², Harry ZEKOLLARI³

¹Earth System Science & Departement Geografie, Vrije Universiteit Brussel, Brussels, Belgium

²Georges Lemaître Center for Earth & Climate Research, Earth and Life Institute, Université catholique de Louvain, Louvain-la-Neuve, Belgium

³Department of Geoscience and Remote Sensing, Delft University of Technology, Delft, Netherlands

**Corresponding author: Lander Van Tricht (lander.van.tricht@vub.be)*

Abstract. The surface mass balance of a glacier (SMB) provides the link between the glacier and the local climate. For this reason, it is intensively studied and monitored. However, major efforts are required to determine the **point** SMB on a sufficient number of locations to capture the heterogeneity of the SMB pattern. Furthermore, because of the time-consuming and costly nature of these measurements, detailed SMB measurements are carried out on only a limited number of glaciers. In this study, we investigate how to accurately determine the SMB in the ablation zone of Vadret da Morteratsch and Vadret Pers (Engadin, Switzerland) using the continuity-equation method, **based on the expression of conservation of mass for glacier flow with constant density. An** elaborate dataset (spanning the 2017-2020 period) of high-resolution data derived from **Unoccupied Aerial Vehicle** (UAV) measurements (surface elevation changes and surface velocities) is combined with reconstructed ice thickness fields (based on radar measurements). To determine the performance of the method, we compare modelled SMB with measured SMB values at the position of stakes. Our results indicate that with annual UAV surveys, it is possible to obtain SMB estimates with a mean absolute error **smaller than 0.5 meters** of ice equivalent per year. Yet, our study demonstrates that to obtain these accuracies, it is necessary to consider the ice flow over spatial scales of several times the local ice thickness, **accomplished in this study by applying an exponential decay filter.** Furthermore, our study **highlights** the crucial importance of the ice thickness, which must be sufficiently well known in order to **accurately** apply the method. The latter currently seems to hamper the application of the continuity-equation method to derive detailed SMB patterns on regional to global scales.

1 Introduction

The surface mass balance of a glacier is determined by the processes adding mass to the surface (e.g. snow fall, freezing rain), and those removing mass from the surface (e.g. snow and ice melt, sublimation). These processes are strongly driven by the **energy budget** and precipitation over the glacier. As a result of increased global mean temperatures, SMBs are becoming increasingly negative, leading to an unprecedented shrinkage of glaciers during the last decade (Zemp et al., 2019; Wouters et al., 2019). Because of the direct link with the local climatic signal, determining the glacier surface mass balance and its distribution is crucial to monitor, understand and model the reaction of glaciers to climate change. Traditionally, a stake and snow pit network are used to determine the SMB followed by an **interpolation and extrapolation** to obtain the glacier **mean** specific mass balance (Braithwaite, 2002). This can result in large errors for glaciers where the heterogeneity of the SMB cannot be captured sufficiently by the available measurements (Zemp et al., 2013). Further, because of the time-consuming and costly nature of these measurements, detailed SMB measurements are carried out on only a limited number of glaciers.

Geodetic methods provide an alternative, and have been applied **since many decades** in numerous studies, to monitor mass balances for individual glaciers at local to regional scales (e.g. Brun et al., 2017; Davaze et al., 2020; Sommer et al., 2020). These methods all involve comparing digital elevation models (DEMs), mainly created using airborne and satellite data, over a given period to determine local elevation changes. These local elevation changes result from an interaction between mass balance and ice flow processes and do therefore not allow to directly determine the mass balance distribution over glaciers (Berthier and Vincent., 2012). However, having such a mass balance distribution over glaciers is of large interest, as this can be used to accurately calibrate mass balance models used in large-scale glacier modelling efforts to allow for example for an accurate calibration of mass balance gradients (Zekollari et al., 2018; Marzeion et al., 2020).

Several studies have attempted to determine patterns of SMB from surface elevation changes by implementing either mass-continuity, a kinematic boundary condition at the surface or through 3D ice flow modelling (Kääb and Funk, 1999; Gudmundsson and Bauder, 1999; Hubbard et al., 2000; Reeh et al., 2002; Nuimura et al., 2011; Vincent et al., 2016; Brun et al., 2018; Bisset et al., 2020; Wagnon et al., 2021; Miles et al., 2021). In essence, these are all based on the principle of combining surface elevation changes with the ice flux divergence. While the former can be measured directly, the latter is calculated by combining various types of measurements. Most of previous studies stumbled on the necessity, resulting from the discretization of ice flow processes and spatial resolution of the data, to smooth the input data or the ice flux divergence or to resample to much lower resolutions of several hundreds of metres. **Other studies used cross-sectional flux gates to simplify the problem and calculate a uniform flux divergence across a glacier area downstream of such a flux gate or between two flux gates (Berthier and Vincent., 2012; Vincent et al., 2016).** Further, a recurring drawback in previous studies attempting to detect local and small-scale variations of the SMB was the lack of satellite observations with a sufficiently high spatial and temporal resolution (Ryan et al., 2015). However, with the emergence of UAVs, it turned out to be possible to detect small scale variations at unprecedented centimetre resolution. **Accordingly, several studies have been conducted to derive surface velocities from repeated UAV surveys (Immerzeel et al., 2014; Ryan et al., 2015; Kraaijenbrink et al., 2016; Rossini et al., 2018; Benoit et al., 2019) while other studies focussed on the generation**

of surface elevation changes from multiple UAV surveys, and the comparison with stake measurements (Groos et al., 2019; Yang et al., 2020). In recent years, studies have also attempted to determine the SMB at the location of individual ablation stakes using an UAV and with measured vertical velocities (e.g. Vincent et al., 2021). However, to our knowledge, no research has yet been carried out to derive a transferable method to determine the SMB distribution over an entire ablation zone using multiannual UAV measurements. Furthermore, the optimal ways to calculate the ice flux divergence, and how to represent the spatial scales over which ice flow occurs without resampling to a much lower resolution, remain a topic of discussion.

The aim of this study consists of deriving and applying a method to determine the SMB in the entire ablation zone of two glaciers by combining UAV acquired 3D data and ice thickness measurements through the continuity-equation method. We pay particular attention to the spatial scales that need to be considered in this framework and how these influence the modelled SMB. The performance is evaluated through an in-depth comparison with measured SMB at stakes. To allow the method to be applied for other glaciers, with different data availability, we also perform a comprehensive uncertainty analysis, from which we determine which data is crucial in the application of the method and its accuracy.

2 Study area and fieldwork

The current study focuses on the Morteratsch - Pers glacier complex situated in the Bernina massif in the south-eastern part of Switzerland (European Alps) (Figure 1). Vadret da Morteratsch, with a current length of approximately 6 km, is the main glacier and flows from the south to the north. Vadret Pers, which flows towards Vadret da Morteratsch from the southeast, became a separate glacier in 2015, when both glaciers disconnected (Zekollari and Huybrechts, 2018). At present, the two glaciers cover an area of about 15 km² with a volume of ca. 1 km³ making it the largest continuous ice area in the Bernina region. Vadret da Morteratsch reached its maximum Little Ice Age (LIA) extent between 1860 and 1865 (Zekollari et al., 2014). Since 1878, the glacier front has retreated more than three kilometres and is nowadays located at an altitude of 2200 m above sea level (a.s.l.). The peculiar shape of the front of the Vadret da Morteratsch is caused by a combination of a large amount of debris on the western side that kept the ice below more insulated during the past years, and shading effects from the surrounding mountains. Since the 2000s, the front of the glacier has retreated significantly, but a large area of stagnant ice remained protruded to the north on the western side of the valley (Figure 1). The upper parts of the glacier complex reach 4000 m a.s.l, originating at peaks such as Piz Bernina and Bellavista (Figure 1). The glacier complex has been studied and monitored intensively with SMB stake measurements performed annually at the end of the ablation season since 2001 (Zekollari and Huybrechts, 2018). In addition, the geodetic mass balance of the 1980-2010 period was determined to be between -0.7 and -0.8 metre water equivalent per year (Fischer et al., 2015). The SMB stake measurements served to calibrate a mass balance model (Nemec et al., 2009) which was coupled to a higher-order ice flow model to simulate the future evolution of the glacier complex (Zekollari et al., 2014) and to study its response time (Zekollari and Huybrechts, 2015). Furthermore, the ice thickness in the ablation area has been measured twice (Zekollari et al., 2013; Langhammer et al., 2019) and again in 2020 for specific parts of Vadret da Morteratsch.

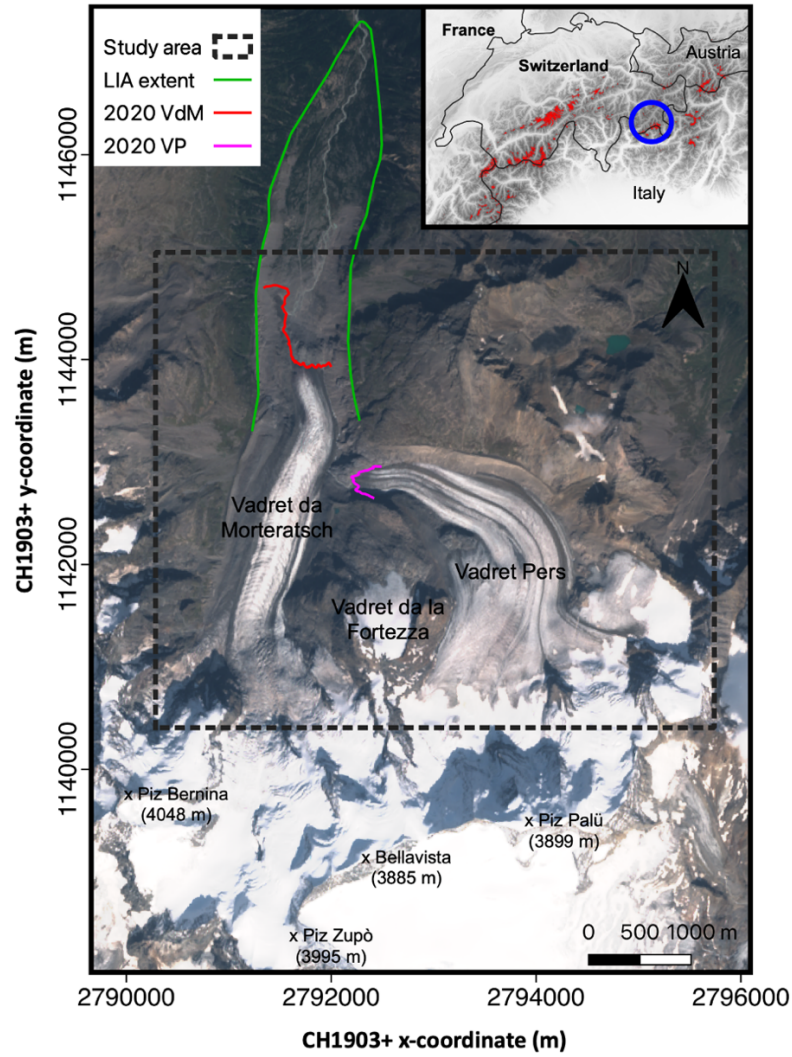


Figure 1. Map of the Morteratsch-Pers glacier complex in southeastern Switzerland. The different coloured lines represent the extent of the glacier at the end of the Little Ice Age (LIA, 1860-1865) and in 2020. The background image is a Sentinel-2 true colour composite satellite image from 13 September 2020. The highest mountains are labelled and indicated with a black cross. The inset shows a DEM of the Shuttle Radar Topography Mission (SRTM) and boundaries of the countries of the central and western European Alps. The areas indicated with a red colour are glaciers according to the Randolph Glacier Inventory (RGI) version 6. The location of the Morteratsch-Pers glacier complex is indicated with a blue circle.

2.1 UAV surveys

Between 2017 and 2020, we conducted annual UAV surveys at the end of the ablation season (late September). Hence, the focus in this research is on three mass-balance years (2017-2018, 2018-2019 and 2019-2020). In 2017, above normal snow cover and severe weather conditions prevented drone mapping on the upper parts of the ablation area of Vadret Pers (>2800 m) due to inadequate visual content for accurate keypoint detection (Gindraux et al., 2017), and the inability to distribute control points. This resulted in a smaller study area in 2017-2018. The observations consist of images acquired by repeated UAV surveys with a DJI Phantom 4 Pro (P4PRO) (in 2017,

2018 and 2019) and a DJI Phantom 4 RTK (P4RTK) (in 2020) quadcopter, both equipped with a 20-megapixel camera. For flight planning and UAV piloting, DJI GS Pro was used. The flight plans were designed to limit the variation in ground sampling distance (GSD) by flying parallel to the main surface slope and by subdividing the study area into smaller sections. We ensured in every case sufficient overlap between the different flight plans so that they could be easily attached to each other afterwards. Additional technical details of the flights are given in Table 1. The different flights within one field campaign were performed on multiple days. However, because of the short fieldwork periods (4-6 days), the difference between the SMB measurements and surface elevation changes caused by not surveying simultaneously is estimated to be at most up to 10 centimeters, which is within the uncertainty bounds of the measurements. Therefore, no correction was applied for the difference in acquisition dates.

Table 1. Technical details and characteristics of the UAV flights.

Setting / characteristic	Value
Flight height above the surface	On average 180 m
Ground resolution	0.05-0.09 m
View angle	90°
Flight speed	5 m/s
Capture interval	4 s
Frontal overlap	90%
Side overlap	70%
Surveyed area (2020)	14.5 km ²
Number of images (2020)	8107
Average number of keypoints / image	65000-70000
Average matched keypoints / image	32000-36000

To ensure sufficient horizontal and vertical accuracy, ground control points (GCPs) were distributed over the area of interest (see Figure 2). The GCPs, plastic orange squares of 40x40 cm, were measured with a Trimble 7 GeoXH RTK GPS (horizontal average accuracy of 0.10-0.20 m, vertical average accuracy of 0.20-0.30 m) by relying on the Swiss Positioning Service (swipos) GIS/GEO. The GCPs were spread over different locations on the glacier following density and distribution guidelines from the literature (Tahar et al., 2012; Goldstein et al., 2015; Long et al., 2016; Tonkin et al., 2016; Gindraux et al., 2017). We ensured homogeneous distribution in almost every case, except where crevasses, moulins or a fresh layer of snow (especially in 2017) impeded this with an average density of 10-20 GCPs km⁻². Specific attention was paid to the distribution of GCPs in the overlapping areas of the different flight areas in order to be able to georeference two neighbouring flight areas with the same points. In 2020, a smaller number of GCPs was placed because the P4RTK can achieve centimetre-level accuracy without a large number of GCPs as a result of an on-board differential GPS system (Zhang et al., 2019; Kienholz et al., 2020). Each year, some of the GCPs (typically 20%) were not used for the georeferencing process, but as a ground validation point (GVP) to assess the quality of the reconstructed DSM.

2.2 In situ surface mass balance data

A total of 287 annual mass balance stake measurements (158 on Morteratsch, 129 on Pers) were performed between 2001 and 2020 in the ablation area of the glacier complex, with an average number of 15 stakes in each year. All the stakes were located between 2100 and 2600 m a.s.l. on the Morteratsch glacier's ablation tongue and between 2450 and 3050 (approximately the ELA) on Vadret Pers. Zekollari and Huybrechts (2018) summarized these measurements and found the SMB rate on Pers glacier to be significantly lower (-2.1 to -2.5 meters of ice equivalent (m i.e.) yr^{-1}) compared to Vadret da Morteratsch at similar elevation. This has been mainly attributed to differences in orientation and the associated daily insolation cycle over the two glaciers. For the period of concern in this study (2017-2020), SMB measurements from 16 individual stakes (8 on each glacier) are available for every year on the debris-free part of the ablation areas (Figure 2). The stakes were measured, and replaced if necessary, annually at the end of each ablation season, during the UAV surveys.

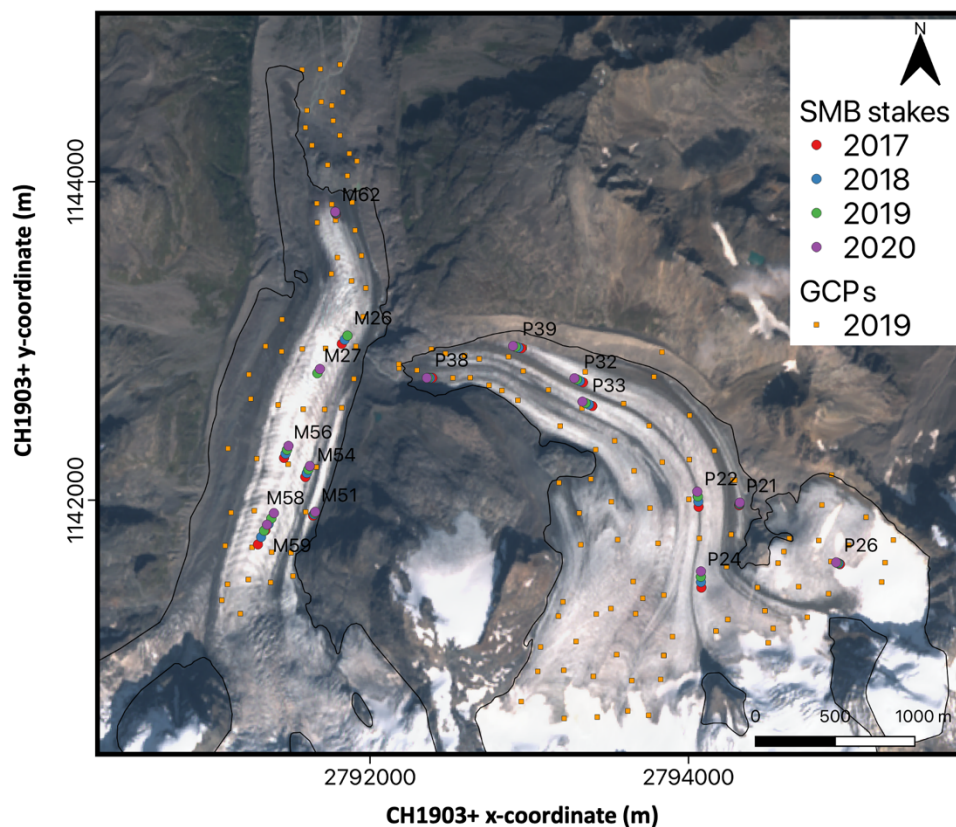


Figure 2. Satellite image of the study area with the location of the measured ablation stakes in 2017, 2018, 2019 and 2020. The GCPs of 2019 are indicated with an orange square. The background image is a Sentinel-2 true colour composite satellite image from 13 September 2020. The different locations of the stakes in 2017-2018-2019-2020 show the movement of the stakes with the glacier flow. The labels refer to the stake names as used in the fieldwork programme. In 2019, stake M26, which was located in the middle of a crevasse field, was replaced by stake M27.

2.3 Ice thickness data

To calculate the local ice volume flux divergence (see section 3.4), a distribution of the ice thickness is required. There are two published datasets of the ice thickness of the Morteratsch – Pers glacier complex, derived from radar measurements (especially in the ablation area) and modelling (especially in the accumulation area). The first one is the dataset of Zekollari et al. (2013), hereafter referred to as THIZ. This distribution was reconstructed by combining measured ice thicknesses (~30 ground borne GPR profiles in the early 2000s) with different modelling constraints. The second ice thickness distribution is the dataset of Langhammer et al. (2019), hereafter referred to as THIL. This distribution was produced by combining measured ice thicknesses (41 helicopter borne GPR profiles with a total of 53247 points measured in 2017) and modelling constraints with the Glacier Thickness Estimation (GlaTE) inversion scheme (Langhammer et al., 2019). We correct both datasets for glacier geometry changes to refer to the glacier state in 2018, 2019 and 2020 respectively by subtracting the amount of local surface lowering. This concerns the local height difference between the UAV created DSMs of 2018-2019-2020 and the DEM used for the respective ice thickness datasets. The latter are two DEMs provided by SwissTopo: DHM25 valid for 1991 (used for THIZ) and SwissALTI3D valid for 2015 (used for THIL).

Although both ice thickness distributions (Figure 3a and Figure 3b) have a similar pattern (location of overdeepenings, location of maximum ice thickness), large local differences exist (Figure 3d). The ice thickness maximum, corrected to represent the ice thickness in 2020, for instance occurs at a similar location but is about 310 m for THIZ and 250 m for THIL. This corresponds to a difference of 18-24% which is however still within the error bounds of the datasets. Conversely, there are also certain zones (especially higher up Vadret da Morteratsch) where the difference between the two datasets is about 150 metres.

Because of the significant differences between both ice thickness distributions, the choice for a particular distribution has a considerable effect for the calculations in this study. To verify the maximum ice thickness of Vadret da Morteratsch, we measured the ice thickness once again in the thickest region in 2020 with a Narod Radio Echo Sounding (RES) system, similar to Zekollari et al. (2013) and Van Tricht et al. (2021). We preferred to use a low frequency of 5 MHz to limit the amount of attenuation due to disturbances in the glacier such as water inclusions, repeatedly observed during the fieldwork. We found a maximum value of 296 metres which is relatively close to the maximum thickness from the THIZ dataset. We can therefore certainly not ignore this dataset, despite the smaller number of measurements and the older date of creation. Therefore, for further calculations, we decided to use the mean ice thickness from THIZ and THIL at every grid cell, hereafter referred to as THIA (Figure 3c). The effect of using THIA, as opposed to relying on THIZ or THIL, is examined as a part of the sensitivity analysis (see section 5.1). For the areas where the current elevation is lower than the bedrock inferred from THIZ and THIL, and where there is no ice as a result within the current glacier outline, we assume a minimal ice thickness of 5 m as in Zekollari et al. (2013).

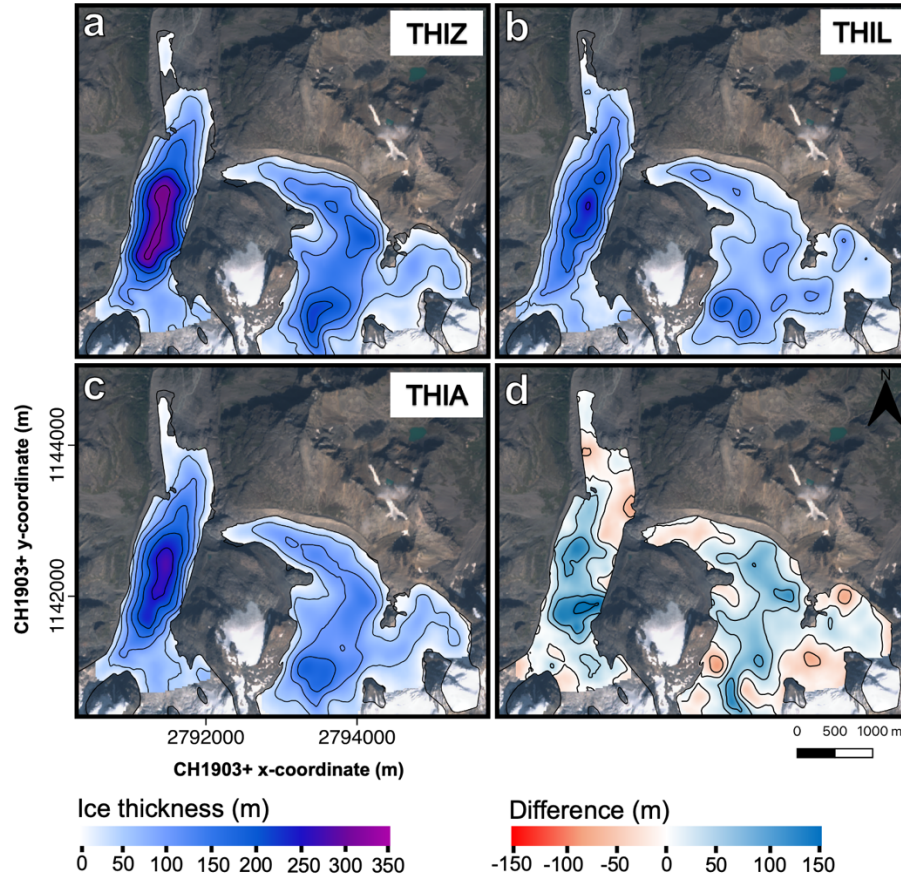


Figure 3. Ice thickness distribution of the ablation area of the Morteratsch-Pers glacier complex in 2020. (a) THIZ (ice thickness distribution of Zekollari et al. (2013)), (b) THIL (ice thickness distribution of Langhammer et al. (2019)) and (c) THIA (average ice thickness distribution). The difference between THIZ and THIL is shown in panel d. Contour lines represent 50 m intervals. Note that at the front of Vadret da Morteratsch and locally at the front of Vadret Pers, the glacier outline is larger than the ice thickness dataset. The current surface elevation of these areas is lower than the bedrock elevation inferred from THIL and THIZ. The background image is a Sentinel-2 true colour composite satellite image from 13 September 2020.

3 Methods

3.1 Continuity-equation method

The continuity equation for glacier flow with constant density (Eq. 1) links the local mass balance (b) and the ice flux divergence per unit width in the local vertical ice column ($\nabla \cdot \vec{q}$) with local changes in the ice thickness ($\frac{\partial H}{\partial t}$), all expressed in m i.e. yr^{-1} (see e.g. Hubbard et al., 2000; Berthier and Vincent, 2012).

$$\frac{\partial H}{\partial t} = b - \nabla \cdot \vec{q} \quad (1)$$

Eq. 1 shows that the difference between the local mass balance and ice flux divergence must be compensated by a change in local ice thickness. If the bedrock elevation is assumed to be constant and compaction is negligible, which is the case in the ablation area (with ice throughout the entire column), the local ice thickness (H) in Eq. 1 can be replaced by the elevation of the surface (h). Further, **because** basal and internal mass balance in the ablation area are predominantly much smaller compared to the surface mass balance (b_s) (Kaser et al., 2003; Huss et al., 2015), b can be replaced by b_s , which after a reorganisation leads to the following expression:

$$b_s = \frac{\partial h}{\partial t} + \nabla \cdot \vec{q} \quad (2)$$

By determining the local elevation changes (section 3.2) and the components that make up for the ice flux divergence per unit width (from now on referred to as ice flux divergence; sections 3.3-3.4), the SMB pattern can then be derived.

3.2 DSM generation and surface elevation changes ($\partial h / \partial t$)

First, all the data from the UAV surveys are used to generate DSMs on a common local coordinate system (**CH1903+ LV95**). All the images collected during the UAV surveys are processed into orthophotos and DSMs using the photogrammetry workflow implemented in Pix4D. The accuracy of the reconstructed DSMs is assessed using the GVPs **and the stable terrain outside the glacierized areas**. Subsequently, surface elevation changes are directly computed from these DSMs by subtracting the DSMs from each other (2018-2017, 2019-2018, 2020-2019). Initially, all the DSMs are generated with a very high resolution of 0.05-0.09 m. But eventually, the surface elevation changes are resampled to 25 m resolution for further calculations using a block moving average filter. This corresponds to the resolution of the ice thickness datasets and will therefore be the grid size for all of the following calculations.

A commonly observed feature on surface elevation change maps derived from high resolution DSMs are alternating positive and negative differences. These are caused by the advection of local glacier topography such as crevasses, moulins, **supraglacial melt streams**, and large ice or rock boulders (Figure 4) (Brun et al., 2018; Rounce et al., 2018; Yang et al., 2020). The above-mentioned variations are not caused by reduced or increased melt or accumulation and therefore **need to be corrected for ice flow** to make a correct SMB estimate.

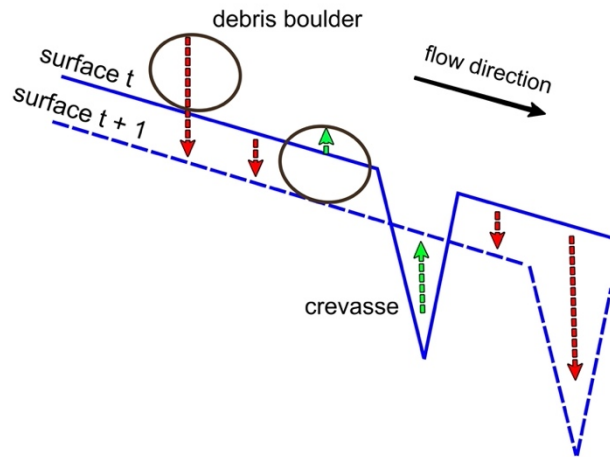


Figure 4. The advection of surface topography (such as debris boulders and crevasses) can alter surface elevation changes between timestep t and $t+1$ (red = negative $\partial h/\partial t$, green = positive $\partial h/\partial t$). The net effect on the surface elevation depends on the amount of lowering and the vertical extent of the moving features on the glacier surface.

The different DSMs are treated considering the motion of the ice, following the method applied in e.g. Brun et al. (2018). This method consists of projecting each point on the glacier back to its original position in the previous year, based on the local velocity in x and y direction and taking into account the vertical displacement produced by flow along the longitudinal slope. The latter is determined by taking the average slope over all the different years for which a DSM was made, smoothed with a Gaussian filter.

3.3 Horizontal surface velocity

Glacier surface velocities, which are needed to calculate the ice flux divergence (section 3.4) and to flow correct the surface elevation changes (section 3.2), are computed for the three individual mass balance years. Velocity grids are derived by applying the Image Geo Rectification and Feature Tracking toolbox (ImGRAFT), an open-source tool in MATLAB (Messerli and Grinsted, 2015). Specific settings for the template matching of ImGRAFT are the use of the orientation correlation (OC) method and a large search height and search width of 200 m, to guarantee that all possible areas are covered. Instead of using visual image data with variable illumination and snow cover, the feature tracking algorithm is run on hillshades (relief DSMs) of the original DSMs resampled to a resolution of 2 m (Messerli and Grinsted, 2015). The latter turned out to improve the correlation success (Rounce et al., 2018).

Velocity maps are computed and corrected for differences in acquisition dates to obtain values in metre per year. Then, a series of filters is applied to the output of the cross-correlation to exclude poorly correlated pixels and those with unrealistic displacements or flow directions (Ruiz et al., 2015). The latter is a common issue for snow

covered areas, debris covered areas or complex crevassed areas where no accurate displacements can be detected. As a first filter, after verifying average zero displacement for stable areas outside the glacier, all the computed velocity vectors outside the glacierized areas are removed by using the digitized glacier outlines (Heid and Kääb, 2012). The latter are manually digitized based on drone and satellite images and correspond to the end of the summer of every balance year under consideration. Then, a median filter is applied which removes velocity components that deviate too much from the surrounding grid cells (Heid and Kääb, 2012; Nagy et al., 2019). Finally, we impose a maximum velocity threshold derived from the modelled velocities in Zekollari et al. (2013), which are constrained with field observations. In other words, we limit the maximum surface velocity at every grid cell to the velocity modelled in Zekollari et al. (2013) + 20%. The latter is a margin to take into account potential errors present in the study of Zekollari et al. (2013). However, after analysis this proved not to be necessary as these high values did not occur. The raw velocity maps containing gaps after filtering are then interpolated using a cubic spline interpolation (Ruiz et al., 2015). As validation, we compare the obtained velocities with measured velocities from stakes.

3.4. Ice flux divergence from ice thickness and surface velocities

The ice flux divergence (in m i.e. yr⁻¹) corresponds to the local upward or downward flow of ice relative to the glacier surface. It represents the difference between the ice supplied from upstream and lost downstream at a particular position. It is defined to be negative for upward motion (mass supplied to the surface, also referred to as the emergence velocity) and positive for downward motion (mass is removed from the surface, also referred to as the submergence velocity).

Different approaches exist to calculate the ice flux divergence ranging from the use of 3D ice flow models (Seroussi et al., 2011; Vincent et al., 2021) to the use of simple geometric calculations and flux gates (Nuimura et al., 2011; Berthier and Vincent, 2012). The important distinction is the simplicity and the resolution with which they can be calculated. In this study, the ice flux divergence is computed for each grid cell, by combining surface velocities and ice thickness according to Eq. 3:

$$\nabla \cdot \vec{q} = F \left(u_{s,x} \frac{\partial H}{\partial x} + u_{s,y} \frac{\partial H}{\partial y} + H \frac{\partial u_{s,x}}{\partial x} + H \frac{\partial u_{s,y}}{\partial y} \right) \quad (3)$$

The right side of Eq. 3 contains two horizontal ice flux components of which the first corresponds to the ice thickness divergence and the second one to the velocity divergence (Reeh et al., 2003). Both are computed from the relevant derivatives. F is the depth averaged glacier velocity ratio (\bar{u}/u_s). For an isothermal glacier, with negligible basal sliding and Glen's flow coefficient $n = 3$, F is 0.8. However, the Morteratsch-Pers glacier complex is assumed to be a temperate alpine glacier complex which is accompanied by basal sliding. According to Zekollari et al. (2013), internal deformation accounts glacier wide on average for 70% of the flow and basal sliding for the remaining 30%. However, in the ablation area the contribution of internal deformation is most likely even higher.

Therefore, for the standard runs in this study, we take an F-value of 0.9. However, the F-value may vary locally (Zekollari et al., 2013) and varying this parameter will therefore be part of the sensitivity analysis.

3.4 Spatial scales of the ice flux divergence

In contrast to the surface elevation changes, for which the accuracy is expected to be high, the computed ice flux divergence is subject to larger uncertainties. This uncertainty directly relates to the large uncertainties in the reconstructed ice thickness field. Moreover, a considerable part of the uncertainty also originates from the spatial scales that need to be considered: due to longitudinal stresses, the local ice dynamics do not only depend on the local glacier geometry (an assumption of the Shallow Ice Approximation, see e.g. Hutter and Morland (1984)), but also on the surrounding geometry, typically over scales corresponding to several times the local ice thickness (accounted for in higher-order and Full Stokes models, see e.g. Zekollari et al. (2014), where such a model was applied for this glacier complex). Local gradients of the ice thickness and the velocity are often magnified when they are determined on a numerical grid with a central difference scheme. This is directly reflected in the ice flux divergence pattern. Therefore, to make the ice flux divergence solution independent of the resolution and to take non-local stresses into account, larger scales must be considered (Reeh et al., 2003; Rounce et al., 2018). **To date, studies applying the continuity equation method, usually resampled the ice flux divergence grid to a much lower resolution (Nuimura et al., 2011; Seroussi et al., 2011; Rounce et al., 2018) or considered a flux gate approach (Berthier and Vincent., 2012; Vincent et al., 2016; Brun et al., 2018).** However, as we aim for a high resolution of the SMB determination in this study **and to obtain spatial variations in the ice flux divergence field**, we opt to retain the 25 m resolution and to consider larger scales for the calculation of the ice flux divergence.

Different filters have been applied, of which most are constant box filters (e.g. mean, median) with a strong variation in size (up to 10000 metres) (Kääb and Funk, 1999; Seroussi et al., 2011; Rounce et al., 2018). Such filters give equal weights to cells within the box irrespective of their distance from the point in consideration (Kamb and Echelmeyer, 1986; Le Brocq et al., 2006). **In this way, the effects of local phenomena (such as an ice fall or an acceleration in the glacier flow) are spread out uniformly when these filters are applied over larger distances, which implies that there are no localized peaks in the flux divergence field.** Also, these filters have an abrupt cut-off point where the weighting becomes zero (Le Brocq and others, 2006). Furthermore, effects of perturbations in for example ice thickness have been demonstrated to fade out exponentially for ice flow (Kamb and Echelmeyer, 1986). Because of all these reasons, we apply **in this study** a local exponential decay filter (Eq. 4):

$$\nabla \cdot \vec{q}_{[x,y]} = \sum_{i=-\text{dist}}^{\text{dist}} \sum_{j=-\text{dist}}^{\text{dist}} W_{[x+i,y+j]} \nabla \cdot \vec{q}_{[x+i,y+j]} \quad (4)$$

In Eq. 4, dist is the maximum distance of a cell which is taken into account in the exponential decay filter (set at 2.5 km), i and j are indices, and W represents the weight of a particular cell at position [x+i, y+j] (Le Brocq et al., 2006):

$$W_{[x,y]} = e^{-\frac{1}{sl} \sqrt{(x'-x)^2 + (y'-y)^2}} \quad (5)$$

In Eq. 5, x and y are the coordinates of the point being filtered while x' and y' are the coordinates of the weighted points. sl is the scaling length which is a crucial parameter determining how fast the exponential filter fades. This parameter directly relates to the length scale over which the longitudinal stresses determine the local ice flow. Theoretically, this scaling length is in the range of 1-3 times the local ice thickness for valley glaciers and 4-10 times for ice sheets (Kamb and Echelmeyer, 1986; Le Brocq et al., 2006). For our experiments, we vary the scaling length depending on A times the local ice thickness (Eq. 6). In this way, we incorporate variations within the study area into the exponential decay filter and we account for non-local flow coupling. The latter was shown to be an improvement compared to fixed-size filters (Le Brocq et al., 2006). In this way, the ice flux divergence in areas with a larger ice thickness is considered over a larger distance compared to areas with a smaller ice thickness.

$$sl[x, y] = A * H[x, y] \text{ with } A \in \{0: 1: 10\} \quad (6)$$

To provide for conservation of mass, the filtered result in each grid cell is multiplied by the ratio of the net flux divergence (sum of all ice flux divergences) before and after filtering. To determine the optimal procedure to include the effects of (longitudinal) stresses and uncertainty in the input data, we perform multiple experiments with the exponential decay filter. For this, we examine whether (i) the ice flux divergence, (ii) the gradients of velocity and ice thickness or (iii) both should be considered over larger spatial scales for optimal results in the determination of the SMB.

First, the ice flux divergence is considered over larger spatial scales by applying the exponential decay filter to the ice flux divergence field. Second, to compensate solely for the effects of large gradients, the gradients are considered over larger spatial scales. We therefore apply the exponential filter to the ice thickness and velocity gradients and calculate the ice flux divergence using these smoothed gradients. Third, to compensate for the negative effects of very large scaling lengths for both previous experiments and the biases related to both, we filter twice. Hence, both filters are applied after each other. In this way, the smoothness of the ice flux divergence field increases while the top values are not damped as much as applying a filter once with a long scaling length. This tends to reduce the distance over which the filtering must be performed, which is favourable to preserve local variations.

For every experiment, the modelled and measured SMB values at the position of the stakes are compared (see section 2.2). As metrics to quantify the performance of the procedure, the mean absolute error (MAE) and the root mean square error (RMSE) are used (Eq. 7 and 8). The MAE is defined as the absolute difference between the modelled and the measured SMB. The RMSE on the other hand takes into account the variance of the errors. n is the number of stake measurements. The uncertainty of the SMB measurements is estimated to be ± 0.2 m i.e. yr^{-1} and is also considered in the analysis. More specifically, for each filter option we carry out 100 versions in which we perturb the measured SMB. This is done by randomly adding a value between -0.2 and 0.2 distributed around 0. Then, for the option under consideration, the average MAE and RMSE are calculated from Eqs. 7 and 8, where n is the number of SMB measurements for every year (see section 2.2). i is an index ranging from 1 to n (16), x_i and y_i are the Cartesian coordinates of the different stakes under consideration.

$$\text{MAE} = \frac{1}{n} \left(\left| \sum_{i=1}^n b_{s,\text{modelled}}(x_i, y_i) - b_{s,\text{measured}}(i) \right| \right) \quad (7)$$

$$\text{RMSE} = \sqrt{\frac{\sum_{i=1}^n (b_{s,\text{modelled}}(x_i, y_i) - b_{s,\text{measured}}(i))^2}{n}} \quad (8)$$

4 Results

4.1 Surface elevation changes and filtering

The accuracy of the elevation product is **first** assessed by comparing the photogrammetrically created DSMs with GVPs, randomly selected over the study area. Mean absolute errors (MAE) between measured and modelled elevation are in the order of a few cm (Table 2), which is similar to values found in other studies (Whitehead et al., 2013; Immerzeel et al., 2014; Wigmore and Mark, 2017; Zhang et al., 2019). As such, the accuracy of the created DSMs is high. Furthermore, the mean error (ME) is close to zero which indicates that the created DSMs are not biased. For 2017, the slightly larger MAE is probably caused by a smaller number of GCPs combined with a reduced visual content because of fresh snow on the glacier surface. Further, the small MAE and RMSE of the DSM in 2020 highlight the advantage of using a RTK equipped with an RTK GPS (P4RTK) for which a smaller amount of GCPs is needed to reach similar or better accuracies compared to a classic setup (UAV without RTK correction).

Table 2. Mean absolute error (MAE) and root mean square error (RMSE) of the elevation differences between the DSMs and the GVPs in different years. (Units are in m).

Year	MAE	ME	RMSE	GCP density (km ⁻²)	UAV used
2017	0.09	-0.07	0.16	11	P4PRO
2018	0.06	-0.02	0.22	24	P4PRO
2019	0.08	0.03	0.16	18	P4PRO
2020	0.07	0.03	0.10	11	P4RTK

Then, the accuracy of the surface elevation changes is assessed by comparing the elevation differences in rectangular areas outside the glacierized areas for two regions (see Figure 6), where the topography is assumed to be mostly stable (Yang et al., 2020). The histograms for the three different balance years in consideration show that most of the differences range between -0.2 and 0.2 m, which indicates that there is no large absolute offset between the DSMs of the different years (Figure). For region 2, we find a larger standard deviation (SD) for the 2017-2018 difference which appears to be caused by a small horizontal shift which produces larger elevation differences (both negative and positive) in this steeper area. For the gentler sloping glacier surface, the effects are negligible. The larger SD for the 2019-2020 difference in region 1 is caused by an area where a part of the bare surface was eroded by a melt river, producing a tail of negative elevation differences. In general, the above analysis reveals that the vertical uncertainties resulting from the DSM differencing are limited.

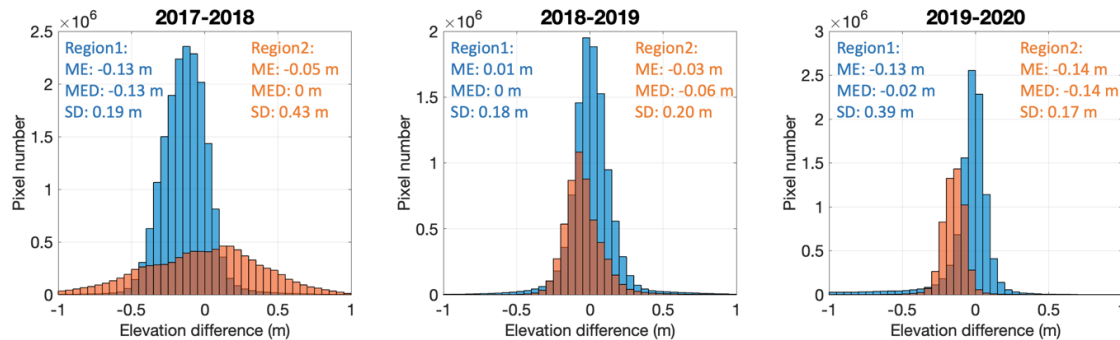


Figure 5. Histograms of elevation differences for the different balance years considered. The mean error (ME), median error (MED), and standard deviation (SD) are added for each region.

The different maps for the three balance years display a very detailed pattern of surface elevation changes (Figure 6). For example, alternating positive and negative surface elevation changes are noticeable and can be explained by the advection of local glacier surface topography due to glacier movement (see also Figure 4). In addition, significant less negative $\partial h/\partial t$ values at the left side of Vadret da Morteratsch, especially where the glacier protrudes towards the north, are likely the result of a debris cover insulating the ice below and decreasing the melting rate (Reznichenko et al., 2010; Rounce et al., 2018; Rossini et al., 2018). The latter was also observed by

the study of Rossini et al. (2018) focussing on the elevation differences on the front of Vadret da Morteratsch in the summer of 2016. Only at the terminal ice cliff, significantly higher $\partial h/\partial t$ values can be observed (Immerzeel et al., 2014). Given that the ice fluxes can be assumed to remain relatively constant over the three years in consideration, the elevation changes indicate that 2017-2018 was the year with the most negative SMB (which is confirmed by field measurements (see Figure 11). Further, large positive surface elevation changes can be distinguished for 2019-2020 at the highest part of Vadret Pers. This is probably the result of avalanches originating from the steep accumulation area and persistent snow cover in these areas. This is striking as surface elevation changes further down on the glacier are generally more negative compared to 2018-2019: i.e. the SMB gradient on Vadret Pers is steeper in 2019-2020 compared to 2018-2019.

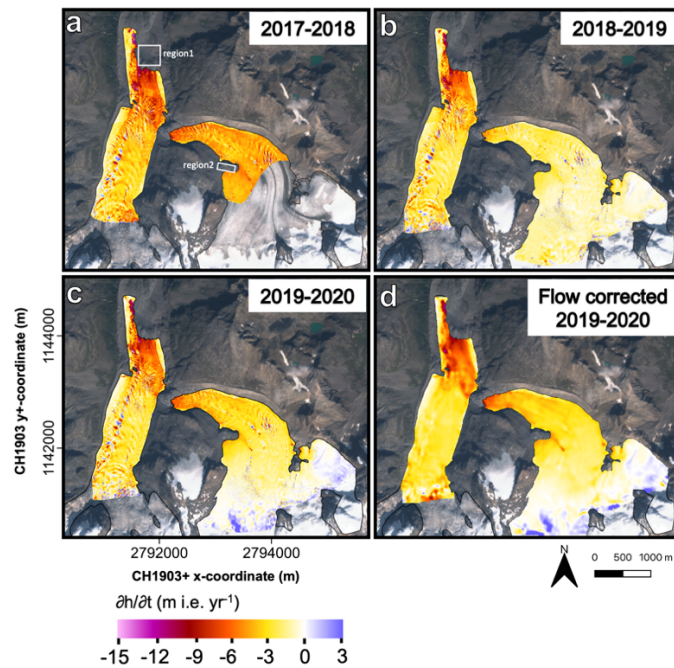


Figure 6. Surface elevation changes for (a) 2017-2018, (b) 2018-2019 and (c) 2019-2020. The spatial resolution is equal to 8 cm. Panel d shows the surface elevation changes for 2019-2020 after flow correction. The outline of the glacier corresponds to the latest year of observation for every balance year in consideration. The two white boxes (region1 and region2) are stable areas which are used for error analysis. The background image is a Sentinel-2 true colour composite satellite image from 13 September 2020.

Alternating positive and negative surface elevation changes are evident, caused by the advection of surface topography (Figure 4 and Figure 6). We correct for these non-SMB features by flow correcting the DSMs (see section 3.2). The alternating pattern has clearly faded (Figure 6d). At the top of the ablation area of Vadret da Morteratsch, near the ice fall, the $\partial h/\partial t$ values at the margin of the area are unrealistic because of inaccurate velocity calculations (see Figure 7) and margin effects of the longitudinal slope. However, this area lies outside the area under investigation (see Figure 7).

4.2 Glacier surface velocity

The velocity map derived from feature tracking and filtered for errors (see section 3.3), contains several voids (Figure 7a). This is caused by a lack of correlation between the two years, which is typically related to deformations of the surface, **repositioning of supraglacial melt streams**, and the presence of snow cover or debris. The latter hampers an accurate tracking between two consecutive years. To fill these gaps, cubic spline interpolation is used (Figure 7b).

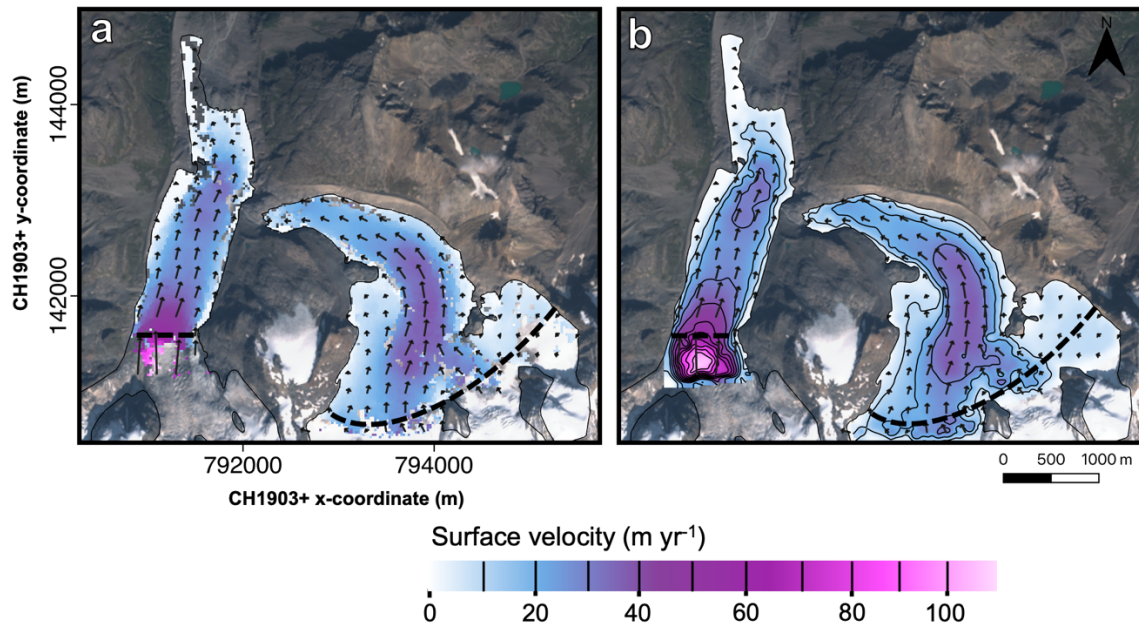


Figure 7. Horizontal surface velocities derived from feature tracking between 2019 and 2020. (a) filtered surface velocity, (b) void-filled filtered surface velocity. The black arrows indicate the flow direction. The dashed black line indicates the limit of the glacier area where the velocity is modelled without many gaps (area used for further analyses, e.g. when calculating ice flux divergences). The background image is a Sentinel-2 true colour composite satellite image from 13 September 2020. The contour lines are added for every 10 m and they are indicated in the colorbar.

Comparison with the velocities obtained by field measurements using ablation stakes (based on high-precision RTK GPS system, estimated accuracy of approx. 0.1 m yr^{-1}) reveals a good agreement. We find the ME and RMSE to be $0.01 / 1.7 \text{ m yr}^{-1}$ for 2017-2018, $0.99 / 1.9 \text{ m yr}^{-1}$ for 2018-2019 and $-0.37 / 1.8 \text{ m yr}^{-1}$ for 2019-2020 (Figure 8).

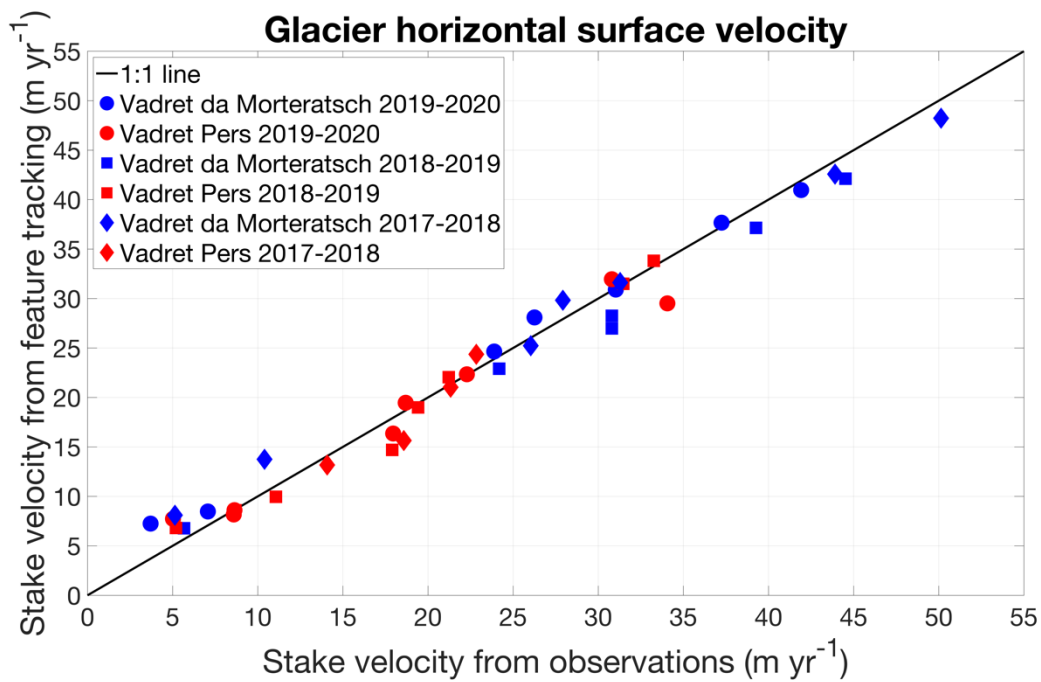


Figure 8. Comparison between surface velocities at stakes from field observations (high precision GPS measurement at stakes) and from feature tracking.

The surface velocities of 2017-2018 are higher compared to 2018-2019. Because the surface velocities in 2019-2020 also appear to be slightly larger compared to 2018-2019, it might be due to a larger amount of basal sliding in these two balance years. The latter can be caused by an increased supply of meltwater lubricating the glacier's base which can be linked to a more negative $\partial h / \partial t$ in 2017-2018 and 2019-2020 compared to 2018-2019 (see also Figure 6).

4.3 Ice flux divergence

After considering various spatial scales and filter procedures to determine the ice flux divergence, we find optimal results (lowest MAE, RMSE and minimal scaling length, see section 5.2) when both filters are applied after each other for a scaling length of $4xH$ to smooth the ice thickness and velocity gradients and a scaling length of $1xH$ to smooth the ensuing ice flux divergence (see section 3.4). These values are close to the theoretical values of the fundamental longitudinal scaling length for valley glaciers, mentioned in Kamb and Echelmeyer (1986). It shows that the data needs to be considered over large spatial scales which implies that the ice flux divergence field must be sufficiently smooth to give accurate results.

The computed ice flux divergence is clearly characterized by negative values over both glacier tongues (Figure 9). This represents horizontal compression and associated vertical extension which is generally expected for ablation areas (e.g. Kääb and Funk, 1999). This horizontal compression translates into an ice supply towards the surface

(emergence velocity), which counters the effect of the negative mass balance on the local ice thickness change (and neutralizes it in case the glacier is in equilibrium with the local climatic conditions). The ice flux divergence reaches a minimum between 500 and 1000 m from the terminus of the Vadret da Morteratsch with values close to $-4 \text{ m i.e. yr}^{-1}$ (Figure 9). In this area, both the ice thickness (Figure 3) and the surface velocity (Figure 7) decrease significantly which leads to large negative gradients and hence upward motion (negative ice flux divergence). It is therefore not surprising that there is a complex pattern of transverse crevasses in this area (see Figure 2). The maximum ice flux divergence at the eastern side of Vadret da Morteratsch near the former confluence area with Vadret Pers is suspicious. This is likely caused by the very large ice thickness gradient **because of the contribution of the underestimated ice thickness in the THIZ dataset**. In this area, the THIZ dataset revealed zero ice thickness because of an overestimation of the bedrock elevation (Figure 3).

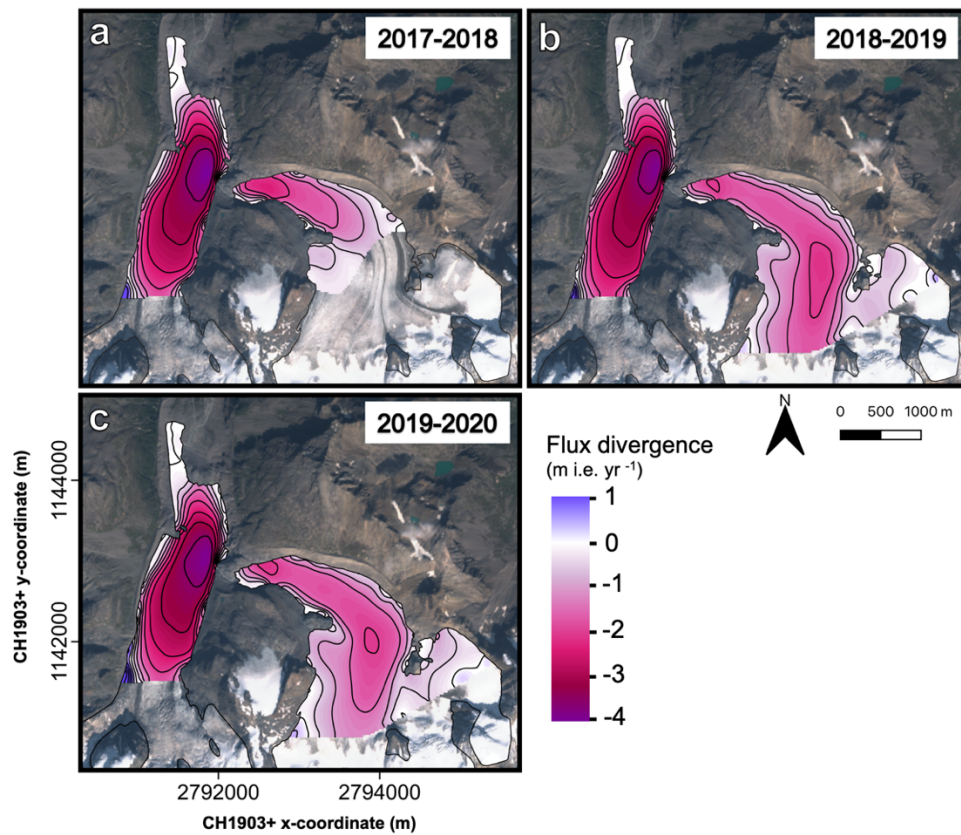


Figure 9. Maps of the modelled ice flux divergence for the different years under consideration. Contours are added for every 0.5 metre per year. The background image is a Sentinel-2 true colour composite satellite image from 13 September 2020.

4.4 SMB from UAV

The final step of the method is to add the surface elevation changes (see Figure 6) and the computed ice flux divergence (Figure 9) to obtain the SMB (see Eq. 1). The final product, the modelled SMB for the three balance

years, is shown in Figure 10. The three years in consideration clearly show a rather similar pattern. Areas with a less negative SMB are located at the same locations (e.g. western margin of Vadret da Morteratsch). Areas with the most negative SMB are also at the same location (e.g. glacier fronts). The ice flux divergence is prominently not able to compensate for the very negative SMB so that there is net mass loss everywhere and the altitude changes are less than zero. The most negative SMB (up to $-13 \text{ m i.e. yr}^{-1}$) is found at the front of Vadret da Morteratsch in 2017-2018 which is in accordance with the SMB measurements. This concerns the lowest area which is also quasi-stagnant with a very limited supply of ice from upstream (see Figure 9). The presence of certain irregular patches with a smaller or larger SMB is caused by artefacts in the flow correction method (see section 3.2 and Figure 6d). This is because the flow correction method cannot trace all displacements exactly (rocks fall over, crevasses deform, supraglacial melt streams are positioned on different locations etc.), and because the velocity field is not fully accurate, and the calculation of the longitudinal slope also affects the result.

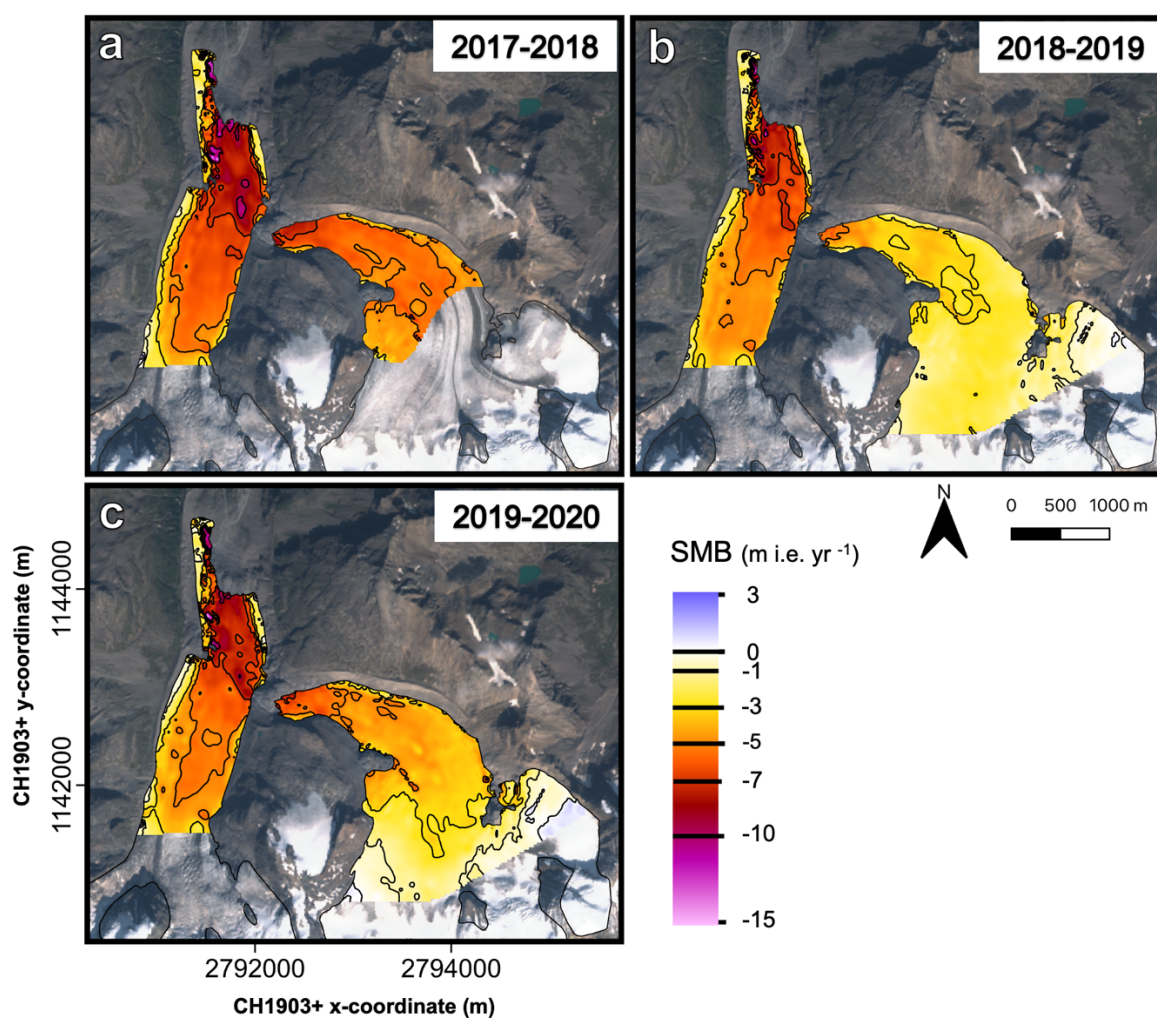


Figure 10. Maps of the modelled SMB fields. Contours are added for specific values (indicated on the colorbar). The background image is a Sentinel-2 true colour composite satellite image from 13 September 2020.

The associated point-by-point comparison between modelled and measured SMB confirms the good match with deviations generally smaller than $0.5 \text{ m i.e. yr}^{-1}$ (Figure 11). The largest differences are found at the front of Vadret Pers (Figure 11). Near the glacier front, the ice flux divergence is likely underestimated as a result of overestimated ice thickness in this area of the THIZ dataset. The latter decreases the ice thickness gradient in this area substantially.

In 2019, stake M26 (see Figure 2) was replaced by M27 (and installed at a higher location) because it was located in the middle of a field of transverse crevasses during the survey in 2019. It is noticeable that this location was characterised by a more negative SMB compared to the surrounding areas in both 2017-2018 and 2018-2019 (see Figure 10 and Figure 11) which is probably caused by a more exposed position on an ice serac.

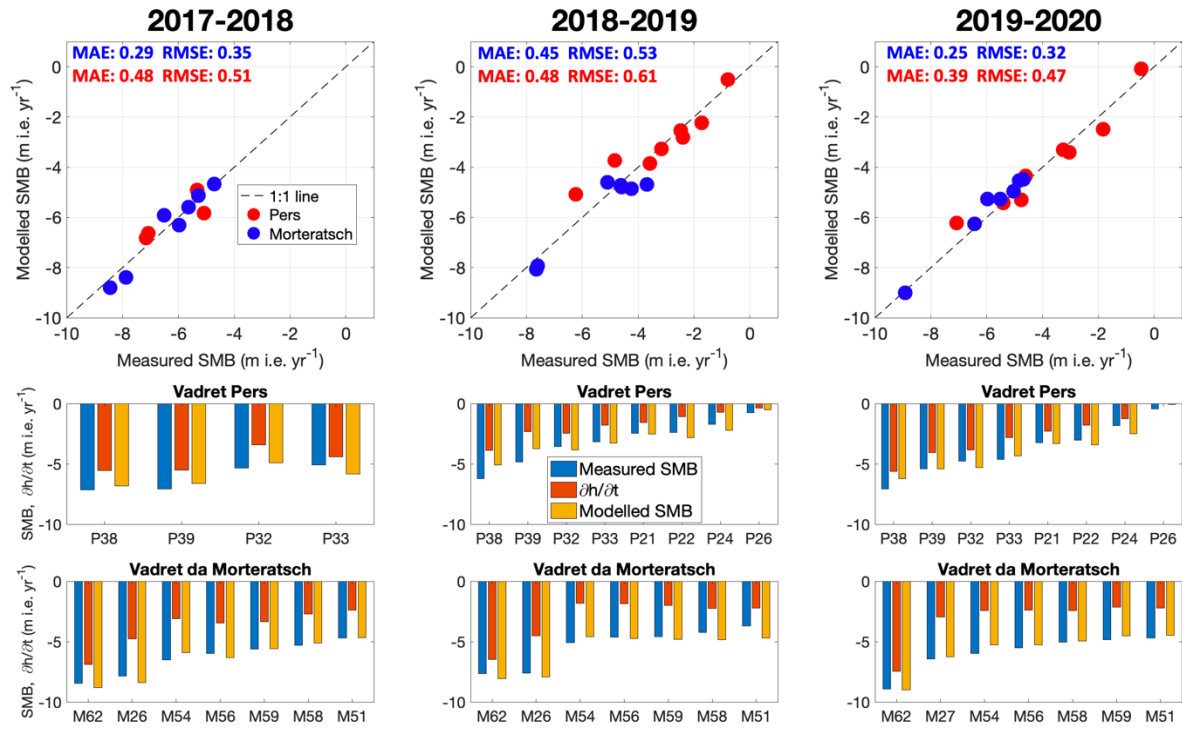


Figure 11. Point-by-point comparison of modelled and measured SMB. In the lower panels, the difference between the modelled SMB (yellow bar) and the local elevation change (red bar) results from the modelled ice flux divergence. The labels refer to the stake names as used in the fieldwork programme. The MAE and RMSE of the modelled SMB are added in the upper panels (Values are in m i.e. yr^{-1}).

For the optimal SMB fields, a minimum MAE of $0.25 \text{ m i.e. yr}^{-1}$ is obtained for Vadret da Morteratsch in 2019-2020 (Figure 11). The MAE and RMSE are somewhat larger for Vadret Pers with a maximum of $0.61 \text{ m i.e. yr}^{-1}$ in 2018-2019 which is mainly caused by the larger deviation for the lowest two stakes (Figure 11).

4.5 Lateral variations in the SMB pattern

Using the continuity method based on close-range (UAV) remote sensing data clearly reveals a much more detailed picture of SMB than is possible from a stake network on a limited number of locations. This is evident in the lateral heterogeneity of SMB, which is often overlooked when considering elevation as the prime variable to plan the stake locations. In Figure 12, the difference is shown between the UAV-derived SMB field and a SMB field only determined by elevation as derived from a linear fit of the stake measurements with altitude (see the inset of Figure 12). In general, the largest differences occur close to the margin of the glaciers, and around their front. The differences at the glacier margin of Vadret da Morteratsch are mainly related to a thick debris cover, which when sufficient in thickness, has an insulating effect that reduces the glacier melt (e.g. Rounce et al., 2018; Verhaegen et al., 2020). For example, for the heavily-debris covered area where Vadret da Morteratsch protrudes towards the north, the SMB is $-1.5 \text{ m i.e. yr}^{-1}$ below the debris and up to $-12 \text{ m i.e. yr}^{-1}$ for the ice next to the debris. **A thin layer of debris, and the terminal ice cliff (Immerzeel et al., 2014), further reinforces the melt here, explaining these very high ablation rate (Rossini et al., 2018).** The melt ratio is accordingly equal to 0.125, which means that there is 87.5% less melt under the debris at this location. This corresponds to a debris thickness of more than 50 cm when a typical average value of the characteristic debris thickness is used (Anderson and Anderson, 2016; Rounce et al., 2018). **Such thicknesses are very likely in this area. During the fieldwork campaigns, boulder supply from the moraines was observed on several occasions, which was also documented in the Himalaya by Van Woerkom et al. (2019).**

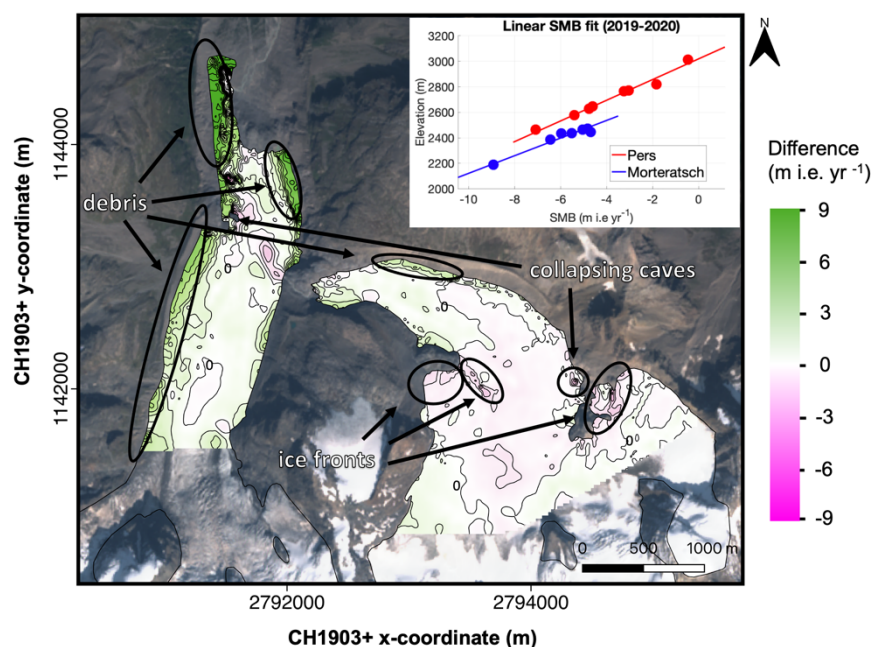


Figure 12. The inset shows a linear SMB fit based on stake measurements. The main figure shows the difference between the UAV-derived SMB and the linearly derived SMB. The background image is a Sentinel-2 true colour composite satellite image from 13 September 2020. Contour lines are added for every metre.

Another major feature is the presence of patches with a clearly more negative SMB when relying on the UAV-derived SMB field. These differences relate to stationary areas at local ice fronts or collapsing ice caves. While the first are real SMB variations (caused by more irradiation and/or less snow), the latter ones are not caused by the SMB. These collapsing ice caves clearly appear to occur near stagnant ice and at the bottom of the glacier where melt water forms a cave below the ice (Figure 12). These caves collapse when the overlying ice becomes too thin due to melting at the surface. For the other areas, the difference between the SMB fields is generally smaller, between -0.5 and 0.5 m i.e. yr^{-1} . This is in the same order as the MAE and the RMSE and is slightly larger than the expected accuracy of the SMB measurements.

5 Uncertainty analysis of the selected data, parameters, and filters

The surface elevation changes and the ice flux divergence contribute separately to the surface mass balance, implying that errors and uncertainties in both terms do not influence each other but directly affect the determined SMB (Eq. 4). It is therefore crucial to determine to which extent the uncertainty of both affects the results of the applied method. In addition, we evaluate the results of the different filter procedures of the ice flux divergence.

5.1 Dependence on the data and F-value used

To study the dependence of the applied method to the uncertainty attributable to the used data and F-value, we create 100 perturbed fields of the surface elevation changes, the surface velocity, the F-value and the ice thickness. After that, we do the calculations, using the perturbed data for one dataset and the original data for the other ones. Next, the MAE of modelled versus measured SMB is calculated 100 times and for all years and the standard deviation of this MAE is determined. For the analysis, the different input fields are perturbed using random patches with a diameter (uniformly distributed) between 50 m (local errors at grid level) and 500 m with perturbation values normally distributed with a standard deviation of half the error estimate. The uncertainty in the surface elevation changes is assumed to be correlated in space, i.e. depending on a pattern across the glacier (e.g. Fisher et al., 2015). Therefore, the $\partial h / \partial t$ fields are perturbed with perturbations of maximum 0.5 m (plausible maximum value for UAV data). Regarding surface velocity, we use error estimates of 10% of the observed velocity, similar to the expected accuracy (see section 4.2). Besides velocity itself, the assumption of a constant F-value is rather unrealistic (Zekollari et al., 2013). Ice flow over basal irregularities causes variations in F. Previous research showed for example F to be larger over basal highs and smaller over basal lows and glacier areas with more basal sliding might as well be characterized by a larger F-value (Reeh et al., 2003). Therefore, we apply perturbations using an F-value between 0.85 and 0.95. Concerning ice thickness, we apply perturbations with an error estimate of 30%, which is mentioned by Zekollari et al. (2013) as an estimate of the accuracy.

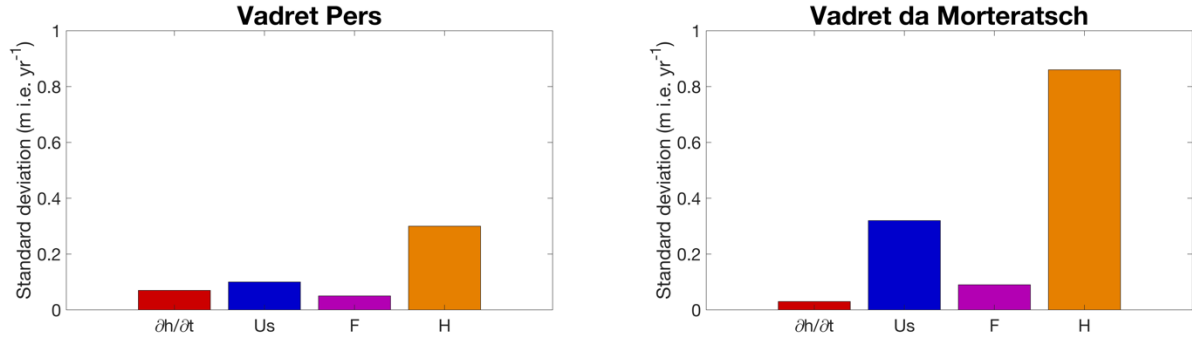


Figure 13. Standard deviation of the MAE for the perturbed versions of the surface elevation changes, the surface velocity (u_s), the F -value and the ice thickness (H).

The effect of perturbation of $\partial h / \partial t$ on the determined SMB is small with a standard deviation of less than 0.1 m i.e. yr⁻¹ for both glaciers (Figure 13). As a result, the results of the applied method are not very dependent on (small) perturbations in $\partial h / \partial t$. Changes in the F -value and surface velocity also appear to have minor contribution, especially concerning Vadret Pers. Regarding Vadret da Morteratsch, the surface velocity has a SD of 0.3 m i.e. yr⁻¹, which is not negligible (Figure 13). The ice thickness distribution, however, is for both glaciers undoubtedly most crucial for the determination of the SMB, and even more so for Vadret da Morteratsch.

We therefore conducted some additional tests with both (THIZ and THIL) individual ice thickness datasets and for different combinations. For Pers glacier, the Langhammer dataset proved to be slightly better, while for Morteratsch, the Zekollari dataset performed better. But in general, all combinations tested gave poorer results, which encouraged us to use the average ice thickness in this study. It should be mentioned that the above analysis is valid for the glacier wide mean SMB deviations. For local point measurements, the uncertainty related to the used data, or the F -parameter, might be larger.

5.2 Evaluation of procedures to filter the ice flux divergence

As the ice flow at a given location is determined by the surrounding glacier geometry (i.e. not only by its local geometry) and to avoid non-physical oscillations in the flux divergence field (as a result of fine grid spacing), it appears to be necessary to consider various spatial scales over which the ice flux divergence needed to be determined and different filtering procedures (see section 3.4). The results of each possible combination are shown in Figure 14.

By only applying the exponential decay filter to the ice flux divergence field (moving down in the matrix), we find minimum MAE and RMSE values when the scaling length is equal to five times H (MAE for Morteratsch-Pers is 0.51 m i.e. yr⁻¹). Such a large scaling length indicates that the ice flux divergence field must be smoothed significantly and therefore becomes entirely smeared with limited variation in the ablation area. One of the reasons for this high value are large ice thickness and velocity gradients resulting from solving ice flow processes on a

high-resolution numerical grid. To compensate for the effects of large gradients, the second option is to consider the gradients over larger spatial scales. We do this by applying the exponential filter to the ice thickness and velocity gradients and calculate the ice flux divergence using these smoothed gradients (moving to the right in the matrix). A minimum MAE of 0.54 m i.e. yr^{-1} is reached as soon as the velocity and ice thickness gradients are considered over six times H . The solution to compensate for the negative effects of a very large scaling length for both previous filters and the biases related to both is to filter twice, as was elucidated in section 3.4 and shown in section 4.3. As soon as the ice thickness and velocity gradients and the ice flux divergence are smoothed, the MAE becomes significantly smaller (Figure 14). The MAE is now much below 1 m i.e. yr^{-1} .

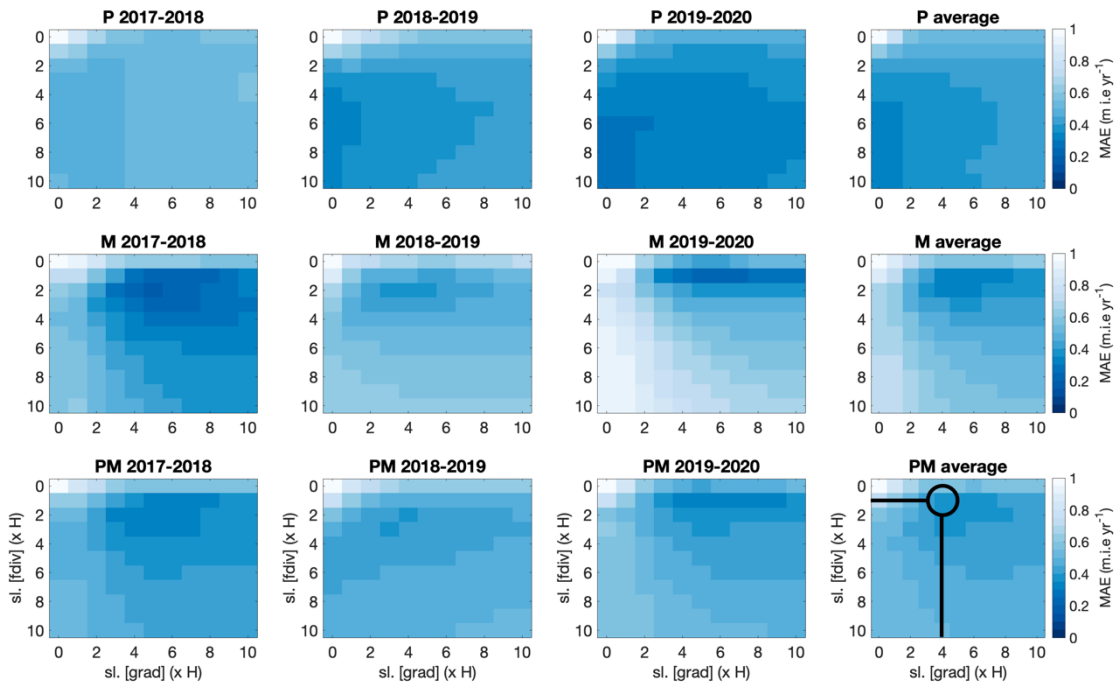


Figure 14. Mean absolute error between measured and modelled SMB for various scaling lengths. The scaling length depends on the local ice thickness ($x H$). Smoothing the ice thickness and velocity gradients (grad) or smoothing the ice flux divergence (fdiv) is represented by the horizontal axis and vertical axis, respectively. M represents Vadret da Morteratsch, P represents Vadret Pers and PM represents the entire glacier complex. The plots entitled with average concern the average over all balance years. The selected combination with which the ice flux divergence is calculated as shown in Figure 9 is encircled with black.

Another observation standing out is that concerning Vadret Pers, the MAE mostly decreases when the ice flux divergence is smoothed while for Vadret da Morteratsch, smoothing the gradients has a larger impact (Figure 14). Our explanation for these peculiar difference is that the gradients (both in terms of ice thickness and surface velocity) for Vadret Pers are already significantly smaller compared to those of Vadret da Morteratsch. The latter glacier has both a higher velocity and a larger ice thickness. Consequently, smoothing of the gradients for Vadret da Morteratsch is more decisive, whereas for Vadret Pers it is the other way around.

Other filters such as a mean filter or a Gaussian filter were explored, but all gave (slightly) less accurate results. However, our tests with a Gaussian filter showed only slightly larger errors for similar spatial scales. A Gaussian filter could therefore be a possible alternative to the exponential filter. Furthermore, the stakes used for validation were not entirely homogeneously distributed throughout the study area. The accuracy analysis may therefore have been biased towards these locations, which may also have influenced the choice of the optimal filter (length).

6 Transferability of the method

Our study shows that with the continuity equation method, the SMB at the position of the stakes can be accurately estimated. It therefore seems to be a promising method for supplementing SMB stake measurements on glaciers. To convert the results presented here to the conventional unit of mass balance, assumptions must be made for density. In the ablation area, to which our study area was limited, the SMB could have been converted directly to metres of water equivalent using an average ice density such as 900 kg/m^3 . However, when the presented method would be applied to for example the accumulation area, specific attention is required for each quantity of the continuity equation (Miles et al., 2021).

The applicability of the method to other, less well studied glaciers, depends on how closely the elevation changes, the surface velocities and the ice thickness can be estimated for these ice bodies. In recent years, a new series of methods have arisen from which surface elevation changes and surface velocities can be rather accurately derived over glaciers (Brun et al., 2017; Paul et al., 2017; Braun et al., 2019; Nagy et al., 2019; Dussaillant et al., 2019; Sommer et al., 2020). This seems encouraging to investigate the applicability using satellite data with a resolution which should preferably be smaller than 10 m for accurate velocity determination. However, our analysis also showed that especially the ice thickness should be known well. So far, the ice thickness has only been measured for less than 0.5% of all glaciers on Earth. As shown in a recent study on four Central Asian glaciers, large-scale thickness estimates may capture the general pattern of the ice thickness distribution and total volume well, yet exhibit significant deviations at the local scale (Van Tricht et al., 2021). To apply the proposed method on glaciers where the ice thickness has not been measured, estimated ice thickness such as the consensus estimate might seem a viable option (Farinotti et al., 2019). To evaluate the use of the consensus estimate, we also computed the SMB using our method and the consensus estimate, for our optimal settings. Concerning Vadret Pers, the MAE and SEE were quite similar while for Vadret da Morteratsch, the MAE and SEE were considerably higher. The latter is likely the result of the ice thickness being significantly too small in the consensus estimate (223 meters while we measured 297 m in 2020). This leaves the question open whether the method can be applied to glaciers where the ice thickness is not measured or known well. Further testing could be performed on other glaciers for which multiannual high-resolution topographic data already exist from repeated UAV surveys (e.g. Immerzeel et al., 2014; Kraaijenbrink et al., 2016; Wigmore et al., 2017; Benoit et al., 2019; Groos et al., 2019; Yang et al., 2020; Vincent et al., 2021).

7 Conclusions

In this study, a method was presented to estimate the surface mass balance pattern from UAV observations, a known ice thickness field, and the principles of mass continuity. Annual surface elevation changes and surface velocities were quantified from UAV and were shown to have centimetre accuracy. The method was applied to the entire ablation zone of Vadret da Morteratsch and Vadret Pers (Switzerland) for three individual balance years between 2017 and 2020. For the well-studied Morteratsch-Pers glacier complex, we were able to closely reproduce SMB surveyed at about 16 stake locations. A major advantage of using close-range (UAV) remote sensing data is that a significantly more detailed SMB pattern can be obtained over the entire ablation area at a high spatial resolution, which is not feasible with a (small) number of stakes. This avoids the need for interpolation and extrapolation from a limited number of stakes, which can introduce several significant errors when the heterogeneity of the glacier surface cannot be captured well from the installed stake positions.

The analysis did not demonstrate a simple consensus on how to consider the ice flux divergence for optimal results on both glaciers. It proved to be necessary to consider large spatial scales concerning the ice flux divergence to apply the continuity-equation method and closely reproduce the SMB at the position of ablation stakes. By using an exponential decay filter to the ice thickness and velocity gradients and the ensuing ice flux divergence over several times the local ice thickness (at least $2x$), the mean absolute error between modelled and measured SMB decreased to 0.25-0.61 m i.e. yr^{-1} for the three balance years. Considering the uncertainty of the data and the stake measurements themselves, this is quite accurate. Our study therefore offers a transferable method that can be used, as long as the ice thickness is sufficiently well known, to estimate the SMB pattern from UAV data. With the increasing resolution of satellite data, we are convinced that the method presented here for UAV data will eventually be able to be used for satellite data as well, allowing it to be easily transferred to other glaciers and regions.

Code and data availability

The model code written in MATLAB, which was used as the basis for this research, can be found and downloaded from <https://github.com/LanderVT/SMB-from-UAV>. The other input datasets and the UAV created DSMs will be provided on request by Lander Van Tricht.

Author contribution

LVT developed the method, performed the experiments, and wrote the manuscript. PH provided guidance in implementing the research and interpreting the results and assisted during the entire process. JVB and AV contributed to the fieldwork, collaborated in developing the method and improved the manuscript throughout the entire process. KVO assisted during the fieldwork and introduced LVT in using UAVs for research purposes. HZ

participated in the fieldwork for many years and contributed throughout the entire process to developing the method and optimising and refining the research.

Competing interests.

The authors declare that they have no conflict of interest.

Acknowledgements

The authors would like to thank Chloë Marie Paice, Felix Vanderleenen, He Zhang, Robbe Neyns, Steven De Hertog, Veronica Tollenaar and Yoni Verhaegen, who assisted during the fieldwork to perform stake measurements and distribute and collect GCPs.

Financial Support

Lander Van Tricht holds a PhD fellowship of the Research Foundation-Flanders (FWO-Vlaanderen) and is affiliated with the Vrije Universiteit Brussel (VUB). Harry Zekollari contributed to the fieldwork as a PhD fellow of the Research Foundation-Flanders (FWO-Vlaanderen) and at a later stage as a Marie Skłodowska-Curie fellow at the TU Delft (grant 799904). K Van Oost is an FNRS Research Director.

Review statement.

This paper was edited by Etienne Berthier and reviewed by Evan Miles, Alexander Raphael Groos, and one anonymous reviewer.

8 References

- Anderson, L.S. and Anderson, R.S.: Modeling debris-covered glaciers: response to steady debris deposition, *The Cryosphere*, 10, 1105–1124, <https://doi.org/10.5194/tc-10-1105-2016>, 2016
- Benoit, L., Gourdon, A., Vallat, R., Irarrazaval, I., Gravey, M., Lehmann, B., Prasicek, G., Gräff, D., Herman, F. and Mariethoz, G.: A high-resolution image time series of the Gorner Glacier – Swiss Alps – derived from repeated unmanned aerial vehicle surveys, *Earth Syst. Sci. Data*, 11, 579–588, <https://doi.org/10.5194/essd-11-579-2019>, 2019
- Berthier, E. and Vincent, C.: Relative contribution of surface mass-balance and ice-flux changes to the accelerated thinning of Mer de Glace, French Alps, over 1979-2008, *Journal of Glaciology*, 58(209), 501-512, <https://doi.org/10.3189/2012JoG11J083>, 2012
- Bisset, R.R., Dehecq, A., Goldberg, D.N., Huss, M., Bingham, R.G. and Gourmelen, N.: Reversed Surface-Mass-Balance Gradients on Himalayan Debris-Covered Glaciers Inferred from Remote Sensing, 12, <https://doi.org/10.3390/rs12101563>, 2020.
- Braithwaite, R.J.: Glacier mass balance: the first 50 years of international monitoring, *Progress in Physical Geography*, 26, 76–95, <https://doi.org/10.1191/0309133302pp326ra>, 2002
- Braun, M.H., Malz, P., Sommer, C., Farías-Barahona, D., Sauter, T., Casassa, G., Soruco, A., Skvarca, P. and Seehaus, T.C.: Constraining glacier elevation and mass changes in South America, *Nature Climate Change*, 9(2), 130–136, <https://doi.org/10.1038/s41558-018-0375-7>, 2019
- Brun, F., Berthier, E., Wagnon, P., Kääb, A. and Treichler, D.: A spatially resolved estimate of High Mountain Asia glacier mass balances from 2000 to 2016, *Nature Geoscience*, 10, 668–673, <https://doi.org/10.1038/ngeo2999>, 2017
- Brun, F., Wagnon, P., Berthier, E., Shea, J. M., Immerzeel, W. W., Kraaijenbrink, P. D. A., Vincent, C., Reverchon, C., Shrestha, D. and Arnaud, Y.: Ice cliff contribution to the tongue-wide ablation of Changri Nup Glacier, Nepal, central Himalaya, *The Cryosphere*, 12, 3439–3457, <https://doi.org/10.5194/tc-12-3439-2018>, 2018
- Davaze, L., Rabatel, A., Dufour, A., Hugonnet, R. and Arnaud, Y.: Region-Wide Annual Glacier Surface Mass Balance for the European Alps From 2000 to 2016, *Frontiers in Earth Science*, 8, 0–14, <https://doi.org/10.3389/feart.2020.00149>, 2020

- Dussaillant, I., Berthier, E., Brun, F., Masiokas, M., Hugonnet, R., Favier, V., Rabatel, A., Pitte, P. and Ruiz, L.: Two decades of glacier mass loss along the Andes, *Nature Geoscience*, 12, 802–808, <https://doi.org/10.1038/s41561-019-0432-5>, 2019
- Farinotti, D., Huss, M., Fürst, J.J., Landmann, J., Machguth, H., Maussion, F. and Pandit, A.: A consensus estimate for the ice thickness distribution of all glaciers on Earth, *Nat. Geosci.*, 1, <https://doi.org/10.1038/s41561-019-0300-3>, 2019
- Fischer, M., Huss, M. and Hoelzle, M.: Surface elevation and mass changes of all Swiss glaciers 1980–2010, *The Cryosphere*, 9, 525–540, <http://doi.org/10.5194/tc-9-525-2015>, 2015
- Gindraux, S., Boesch, R. and Farinotti, D.: Accuracy Assessment of Digital Surface Models from Unmanned Aerial Vehicles’ Imagery on Glaciers, *Remote Sensing*, 9(2), 186, <https://doi.org/10.3390/rs9020186>, 2017
- Goldstein, E.B., Oliver, A.R., deVries, E., Moore, L.J. and Jass, T.: Ground control point requirements for structure-from-motion derived topography in low-slope coastal environments, *PeerJPrePrints* 3:e1444v1, <https://doi.org/10.7287/peerj.preprints.1444v1>, 2015
- Groos, A.R., Bertschinger, T.J., Kummer, C.M., Erlwein, S., Munz, L. and Philipp, A.: The Potential of Low-Cost UAVs and Open-Source Photogrammetry Software for High-Resolution Monitoring of Alpine Glaciers: A Case Study from the Kanderfirn (Swiss Alps), *Geosciences* 9, 1–21, <https://doi.org/10.3390/geosciences9080356>, 2019
- Gudmundsson, G.H. and Bauder, A.: Towards an Indirect Determination of the Mass-balance Distribution of Glaciers using the Kinematic Boundary Condition, *Geografiska Annaler*, 81(4), 575–583, <https://doi.org/10.1111/1468-0459.00085>, 1999
- Heid, T. and Kääb, A.: Evaluation of existing image matching methods for deriving glacier surface displacements globally from optical satellite imagery, *Remote Sensing of Environment*, 118, 339–355, <https://doi.org/10.1016/j.rse.2011.11.024>, 2012
- Hubbard, A., Willis, I., Sharp, M., Mair, D., Nienow, P., Hubbard, B. and Blatter, H.: Glacier mass-balance determination by remote sensing and high-resolution modelling, *Journal of Glaciology*, 46(154), 491–498, <https://doi.org/10.3189/172756500781833016>, 2000
- Huss, M., Dhulst, L. and Bauder, A.: New long-term mass-balance series for the Swiss Alps, *Journal of Glaciology*, 61(227), 551–562, <https://doi.org/10.3189/2015JoG15J015>, 2015

- Hutter, R.K. and Morland, L.W.: Euromech colloquium 172: Mechanics of glaciers, Interlaken, 19–23 September, 1983, Cold Regions Science and Technology, 9(1), 77–86, [https://doi.org/10.1016/0165-232X\(84\)90049-1](https://doi.org/10.1016/0165-232X(84)90049-1), 1984
- Immerzeel, W.W., Kraaijenbrink, P.D.A., Shea, J.M., Shrestha, A.B., Pellicciotti, F., Bierkens, M.F.P. and de Jong, S.M.: High-resolution monitoring of Himalayan glacier dynamics using unmanned aerial vehicles, Remote Sensing of Environment, 150, 93–103, <https://doi.org/10.1016/j.rse.2014.04.025>, 2014
- Kääb, A. and Funk, M.: Modelling mass balance using photogrammetric and geophysical data: a pilot Study at Griesgletscher, Swiss Alps, Journal of Glaciology, 45(151), 575–583, <https://doi.org/10.3189/S0022143000001453>, 1999
- Kamb, B. and Echelmeyer, K.A.: Stress-gradient Coupling in Glacier Flow: IV. Effects of the “ T ” Term, Journal of Glaciology, 32(112), 342–349, <https://doi.org/10.3189/S0022143000012016>, 1986
- Kaser, G., Fountain, A. and Jansson, P.: A manual for monitoring the mass balance of mountain glaciers, International Hydrological Programme (IHP-VI. Technical Documents in Hydrology 59), UNESCO, Paris, 2003.
- Kienholz, C., Pierce, J., Hood, E., Amundson, J.M., Wolken, G.J., Jacobs, A., Hart, S., Wikstrom, Jones K., Abdel-Fattah, D., Johnson, C. and Conaway, J.S.: Deglaciation of a Marginal Basin and Implications for Outburst Floods, Mendenhall Glacier, Alaska. Frontiers in Earth Science, 8, 1–21 <https://doi.org/10.3389/feart.2020.00137>, 2020
- Kraaijenbrink, P., Meijer, S.W., Shea, J.M., Pellicciotti, F., De Jong, S.M. and Immerzeel, W.W.: Seasonal surface velocities of a Himalayan glacier derived by automated correlation of unmanned aerial vehicle imagery, Annals of Glaciology 57, 103–113, <https://doi.org/10.3189/2016AoG71A072>, 2016
- Langhammer, L., Grab, M., Bauder, A. and Maurer, H.: Glacier thickness estimations of alpine glaciers using data and modeling constraints, The Cryosphere, 13(8), 2189–2202, <https://doi.org/10.5194/tc-13-2189-2019>, 2019
- Le Brocq, A.M., Payne, A.J. and Siegert, M.J.: West Antarctic balance calculations: Impact of flux-routing algorithm, smoothing algorithm and topography. Computers and Geosciences, 32(10), 1780–1795, <https://doi.org/10.1016/j.cageo.2006.05.003>, 2006

- Long, N., Millescamp, B., Pouget, F., Dumon, A., Lachaussée, N. and Bertin, X.: Accuracy assessment of coastal topography derived from UAV images, *The International Archives of the Photogrammetry, Remote Sensing and Spatial Information Sciences*, XLI-B1, 1127–1134, <https://doi.org/10.5194/isprs-archives-XLI-B1-1127-2016>, 2016
- Marzeion, B., Hock, R., Anderson, B., Bliss, A., Champollion, N., Fujita, K., Huss, M., Immerzeel, W.W., Kraaijenbrink, P., Malles, J., Maussion, F., Radić, V., Rounce, D.R., Sakai, A., Shannon, S., Wal, R. and Zekollari, H.: Partitioning the Uncertainty of Ensemble Projections of Global Glacier Mass Change, *Earth's Future*, 8(7), 1–25, <https://doi.org/10.1029/2019EF001470>, 2020
- Messerli, A. and Grinsted, A.: Image georectification and feature tracking toolbox: ImGRAFT, *Geoscientific Instrumentation Methods and Data Systems*, 4, 23–34, <https://doi.org/10.5194/gi-4-23-2015>, 2015
- Miles, E., McCarthy, M., Dehecq, A., Kneib M., Fugger S. and Pellicciotti F.: Health and sustainability of glaciers in High Mountain Asia, *Nat Commun* 12, 2868, <https://doi.org/10.1038/s41467-021-23073-4>, 2021
- Millan, R., Mouginot, J., Rabatel, A., Jeong, S., Cusicanqui, D., Derkacheva, A. and Chekki, M.: Mapping Surface Flow Velocity of Glaciers at Regional Scale Using a Multiple Sensors Approach, 11, <https://doi.org/10.3390/rs11212498>, 2019
- Nagy, T., Andreassen, L.M., Duller, R.A. and Gonzalez, P.J.: SenDiT: The Sentinel-2 Displacement Toolbox with Application to Glacier Surface Velocities. *Remote Sensing*, 11(10), 1151, <https://doi.org/10.3390/rs11101151>, 2019
- Nemec, J., Huybrechts, P., Rybak, O. and Oerlemans, J.: Reconstruction of the annual balance of Vadret da Morteratsch, Switzerland, since 1865, *Annals of Glaciology*, 50(50), 126–134, <https://doi.org/10.3189/172756409787769609>, 2009
- Nuimura, T., Fujita, K., Fukui, K., Asahi, K., Aryal, R. and Ageta, Y.: Temporal Changes in Elevation of the Debris-Covered Ablation Area of Khumbu Glacier in the Nepal Himalaya since 1978, *Arctic Antarctic Alpine Research*, 43(2), 246–255, <https://doi.org/10.1657/1938-4246-43.2.246>, 2011
- Paul, F., Bolch, T., Briggs, K., Kääb, A., McMillan, M., McNabb, R., Nagler, T., Nuth, C., Rastner, P., Strozzi, T. and Wuite, J.: Error sources and guidelines for quality assessment of glacier area, elevation change, and velocity products derived from satellite data in the Glaciers_cci project. *Remote Sensing of Environment*, 203, 256–275, <https://doi.org/10.1016/j.rse.2017.08.038>, 2017

- Reeh, N., Mohr, J.J., Krabill, W.B., Thomas, R., Oerter, H., Gundestrup, N. and Bøggild, C.E.: Glacier specific ablation rate derived by remote sensing measurements. *Geophysical Research Letters*, 29(16), 10-1-10-4, <https://doi.org/10.1029/2002GL015307>, 2002
- Reeh, N., Mohr, J.J., Madsen, S.N., Oerter, H. and Gundestrup, N.S.: Three-dimensional surface velocities of Storstrømmen glacier, Greenland, derived from radar interferometry and ice-sounding radar measurements, *Journal of Glaciology*, 49(165), 201–209, <https://doi.org/10.3189/172756503781830818>, 2003
- Reznichenko, N., Davies, T., Shulmeister, J. and McSaveney, M.: Effects of debris on ice-surface melting rates: an experimental study, *Journal of Glaciology*, 56(197), 384–394, <https://doi.org/10.3189/002214310792447725>, 2010\
- Rossini, M., Di Mauro, B., Garzonio, R., Baccolo, G., Cavallini, G., Mattavelli, M., De Amicis, M. and Colombo, R.: Rapid Melting Dynamics of an Alpine Glacier with Repeated UAV Photogrammetry. *Geomorphology*, 304, 159–172, <https://doi.org/10.1016/j.geomorph.2017.12.039>, 2018
- Rounce, D.R., King, O., McCarthy, M., Shean, D.E. and Salerno, F.: Quantifying Debris Thickness of Debris-Covered Glaciers in the Everest Region of Nepal Through Inversion of a Subdebris Melt Model. *Journal of Geophysical Research Earth Surface*, 123(5), 1094–1115, <https://doi.org/10.1029/2017JF004395>, 2018
- Ruiz, L., Berthier, E., Masiokas, M., Pitte, P. and Villalba, R.: First surface velocity maps for glaciers of Monte Tronador, North Patagonian Andes, derived from sequential Pléiades satellite images, *Journal of Glaciology*, 61(229), 908–922, <https://doi.org/10.3189/2015JoG14J134>, 2015
- Ryan, J.C., Hubbard, A.L., Box, J.E., Todd, J., Christoffersen, P., Carr, J.R., Holt, T.O. and Snooke N.: UAV photogrammetry and structure from motion to assess calving dynamics at Store Glacier, a large outlet draining the Greenland ice sheet, *The Cryosphere*, 9(1), 1–11, <https://doi.org/10.5194/tc-9-1-2015>, 2015
- Seroussi, H., Morlighem, M., Rignot, E., Larour, E., Aubry, D., Ben Dhia, H. and Kristensen, S.S.: Ice flux divergence anomalies on 79north Glacier, Greenland, *Geophysical Research Letters*, 38(9), L09501, <https://doi.org/10.1029/2011GL047338>, 2011
- Sommer, C., Malz, P., Seehaus, T.C., Lippl, S., Zemp, M. and Braun, M.H.: Rapid glacier retreat and downwasting throughout the European Alps in the early 21st century, *Nature Communications*, 11(1), 3209, <https://doi.org/10.1038/s41467-020-16818-0>, 2020

- Tahar, K.N., Ahmad, A., Aziz, W.A., Akib, W.M., Mohd, W. and Mohd, N.W.: Assessment on Ground Control Points in Unmanned Aerial System Image Processing for Slope Mapping Studies. *International Journal of Scientific & Engineering Research*, 3(11), 1-10, 2012
- Tonkin, T. and Midgley, N.: Ground-Control Networks for Image Based Surface Reconstruction: An Investigation of Optimum Survey Designs Using UAV Derived Imagery and Structure-from-Motion Photogrammetry, *Remote Sensing*, 8(9), 786, <https://doi.org/10.3390/rs8090786>, 2016
- Van Tricht, L., Huybrechts, P., Van Breedam, J., Fürst, J.J., Rybak, O., Satylkanov, R., Ermenbaiev, B., Popovnin, V., Neyns, R., Paice, C.M. and Malz, P.: Measuring and inferring the ice thickness distribution of four glaciers in the Tien Shan, Kyrgyzstan, *Journal of Glaciology*, 1–18, <https://doi.org/10.1017/jog.2020.104>, 2021
- Van Woerkom, T., Steiner, J. F., Kraaijenbrink, P. D. A., Miles, E. S. and Immerzeel, W.W.: Sediment supply from lateral moraines to a debris-covered glacier in the Himalaya. *Earth Surface Dynamics*, 7(2), 411–427. <https://doi.org/10.5194/esurf-7-411-2019>, 2019
- Verhaegen, Y., Huybrechts, P., Rybak, O. and Popovnin, V.V.: Modelling the evolution of Djankuat Glacier, North Caucasus, from 1752 until 2100 CE, *The Cryosphere*, 14, 4039–4061, <https://doi.org/10.5194/tc-14-4039-2020>, 2020.
- Vincent, C., Wagnon, P., Shea, J.M., Immerzeel, W.W., Kraaijenbrink, P., Shrestha, D., Soruco, A., Arnaud, Y., Brun, F., Berthier, E. and Sherpa, S.F.: Reduced melt on debris-covered glaciers: investigations from Changri Nup Glacier, Nepal, *The Cryosphere*, 10, 1845–1858, <https://doi.org/10.5194/tc-10-1845-2016>, 2016.
- Vincent, C., Cusicanqui, D., Jourdain, B., Laarman, O., Six, D., Gilbert, A., Walpersdorf, A., Rabatel, A., Piard, L., Gimbert, F., Gagliardini, O., Peyaud, V., Arnaud, L., Thibert, E., Brun, F. and Nanni, U.: Geodetic point surface mass balances: a new approach to determine point surface mass balances on glaciers from remote sensing measurements, *The Cryosphere*, 15, 1259–1276, <https://doi.org/10.5194/tc-15-1259-2021>, 2021
- Wagnon, P., Brun, F., Khadka, A., Berthier, E., Shrestha, D., Vincent, C., Arnaud Y., Six D., Dehecq A., Ménégot M. and Jomelli, V.: Reanalysing the 2007–19 glaciological mass-balance series of Mera Glacier, Nepal, Central Himalaya, using geodetic mass balance, *Journal of Glaciology*, 67(261), 117–125, <https://doi.org/10.1017/jog.2020.88>, 2021
- Whitehead, K., Moorman, B.J. and Hugenholtz, C.H.: Brief Communication: Low-cost, on-demand aerial photogrammetry for glaciological measurement, *The Cryosphere*, 7, 1879–1884, <https://doi.org/10.5194/tc-7-1879-2013>, 2013.

- Wigmore, O. and Mark, B.: Monitoring tropical debris-covered glacier dynamics from high-resolution unmanned aerial vehicle photogrammetry, Cordillera Blanca, Peru, *The Cryosphere*, 11, 2463–2480, <https://doi.org/10.5194/tc-11-2463-2017>, 2017.
- Wouters, B., Gardner, A.S. and Moholdt, G.: Global Glacier Mass Loss During the GRACE Satellite Mission (2002-2016), *Frontiers in Earth Science*, 7, 1–11, <https://doi.org/10.3389/feart.2019.00096>, 2019
- Yang, W., Zhao, C., Westoby, M., Yao, T., Wang, Y., Pellicciotti, F., Zhou, J., He, Z. and Miles, E.: Seasonal Dynamics of a Temperate Tibetan Glacier Revealed by High-Resolution UAV Photogrammetry and In Situ Measurements, *Remote Sensing*, 12(15), 2389, <https://doi.org/10.3390/rs12152389>, 2020
- Zekollari, H., Huybrechts, P., Fürst, J.J., Rybak, O. and Eisen, O.: Calibration of a higher-order 3-D ice-flow model of the Morteratsch glacier complex, Engadin, Switzerland, *Annals of Glaciology*, 54(63), 343–351, <https://doi.org/10.3189/2013AoG63A434>, 2013
- Zekollari, H., Fürst, J.J. and Huybrechts, P.: Modelling the evolution of Vadret da Morteratsch, Switzerland, since the Little Ice Age and into the future, *Journal of Glaciology*, 60(224), 1155–1168, <https://doi.org/10.3189/2014JoG14J053>, 2014
- Zekollari, H. and Huybrechts, P.: On the climate–geometry imbalance, response time and volume–area scaling of an alpine glacier: insights from a 3-D flow model applied to Vadret da Morteratsch, Switzerland, *Annals of Glaciology*, 56(70), 51–62, <https://doi.org/10.3189/2015AoG70A921>, 2015
- Zekollari, H. and Huybrechts, P.: Statistical modelling of the surface mass-balance variability of the Morteratsch glacier, Switzerland: strong control of early melting season meteorological conditions, *Journal of Glaciology*, 64(244), 275–288, <https://doi.org/10.1017/jog.2018.18>, 2018
- Zekollari, H., Huss, M. and Farinotti, D.: Modelling the future evolution of glaciers in the European Alps under the EURO-CORDEX RCM ensemble, *The Cryosphere*, 13, 1125–1146, <https://doi.org/10.5194/tc-13-1125-2019>, 2019.
- Zemp, M., Thibert, E., Huss, M., Stumm, D., Denby, C.R., Nuth, C., Nussbaumer, S.U., Moholdt, G., Mercer, A., Mayer, C., Joerg, P.C., Jansson, P., Hynek, B., Fischer, A., Escher-Vetter, H., Elvehøy, H. and Andreassen, L.M.: Uncertainties and re-analysis of glacier mass balance measurements Uncertainties and re-analysis of glacier mass balance measurements, *The Cryosphere Discussions*, 7(2), 789–839, <https://doi.org/10.5194/tcd-7-789-2013>, 2013

1148 Zemp, M., Huss, M., Thibert, E., Eckert, N., McNabb, R., Huber, J., Barandun, M., Machguth, H., Nussbaumer,
1149 S.U., Gärtner-Roer, I., Thomson, L., Paul, F., Maussion, F., Kutuzov, S. and Cogley, J.G.: Global
1150 glacier mass changes and their contributions to sea-level rise from 1961 to 2016, *Nature*, 568, 382–386,
1151 <https://doi.org/10.1038/s41586-019-1071-0>, 2019

1152
1153 Zhang, H., Aldana-Jague, E., Clapuyt, F., Wilken, F., Vanacker, V. and Van Oost, K.: Evaluating the potential
1154 of post-processing kinematic (PPK) georeferencing for UAV-based structure- from-motion (SfM)
1155 photogrammetry and surface change detection, *Earth Surf. Dynam.*, 7, 807–827,
1156 <https://doi.org/10.5194/esurf-7-807-2019>, 2019.